Utrecht University

MASTER THESIS

Modelling the imbibition of an ink-like fluid into the thin coating layer of paper

Author:
Eva SCHOONDERWOERD

First supervisor:
Prof. dr. ir.
Majid HASSANIZADEH

Second supervisor:
Dr.
Hamed ASLANNEJAD

Master Earth Surface and Water
Hydrogeology
Department of Earth Sciences
Faculty of Geosciences

July 9, 2019

UTRECHT UNIVERSITY

Abstract

MSc Earth Surface and Water

Modelling the imbibition of an ink-like fluid into the thin coating layer of paper

by Eva SCHOONDERWOERD

To achieve good results with inkjet printing, it is important to know how an ink droplet will spread over and into a coated paper. In this thesis, a pore-scale and a continuum-scale model are developed to study the infiltration of small droplets into the thin coating layer of paper and to describe the effect of ink properties on this infiltration. With the use of CFD software OpenFOAM, the volume of fluid method is applied for direct pore-scale modelling. The computational domain is constructed with the use of FIB-SEM images of a real paper coating layer. The results are comparable with experimental data. The final ink imprint inside a coating layer is influenced by the droplet position on the coating and the contact angle. Changing the viscosity, density and surface tension has very little effect on the final ink distribution. However, an increase in viscosity and a decrease in surface tension result in a decreased rate of spreading and infiltration. An increase in density results in slightly slower imbibition, while the rate of spreading remains the same. When the droplet arrives at the coating with a velocity of 5 m/s, the rate of spreading and infiltration slightly increases compared to a sessile droplet. Moreover, the wetted area at the paper surface increases slightly in size. HYDRUS is used for continuum-scale modelling. Average hydraulic properties are used to describe the fibrous and coating layer, which means that local differences in pore structure are not incorporated. The results show a large wetted area, containing a large unsaturated region. The results are not comparable with experimental data and the results of OpenFOAM, so pore-scale modelling is a much better option to describe this process.

Acknowledgements

I would like to thank my supervisor, dr. Hamed Aslannejad, for his help and guidance during this research. I also would like my other supervisor, prof. dr. ir. Majid Hassanizadeh for his guidance during this project and his help with choosing a thesis subject. I also thank Bram van der Hoek for his collaboration on the work we did with OpenFOAM. Lastly, I thank prof. dr. ir. Rien van Genuchten for helping me create the HYDRUS models.

Contents

1 Introduction **1**
1.1 Research objectives and thesis outline . . . 3
1.2 Background . . . 4
1.2.1 Printing process . . . 4
1.2.2 Capillary pressure and viscous drag . . . 4
1.2.3 Fluid infiltration . . . 6
1.2.4 Previous studies . . . 7
1.2.5 Pore-scale versus continuum-scale modelling . . . 9
1.2.6 Ink properties . . . 10

2 Methods **11**
2.1 Experimental data . . . 11
2.2 Pore-scale model . . . 12
2.2.1 Equations . . . 12
2.2.2 OpenFOAM structure . . . 13
2.2.3 Meshing . . . 13
2.2.4 Initial conditions . . . 14
2.2.5 Boundary conditions . . . 15
2.2.6 Time settings . . . 15
2.2.7 Model validation . . . 16
2.2.8 Parameter study . . . 16
2.3 Continuum-scale model . . . 17
2.3.1 Equations . . . 17
2.3.2 HYDRUS . . . 18
2.3.3 Geometry and mesh . . . 18
2.3.4 Flow parameters and initial conditions . . . 18
2.3.5 Iteration criteria and time settings . . . 19

3 Results **20**
3.1 OpenFOAM results . . . 20
3.1.1 Model validation . . . 22
3.1.2 Parameter study . . . 24
3.2 HYDRUS results . . . 31
3.2.1 Large droplet . . . 33
3.2.2 Small droplet . . . 34
3.2.3 Coating and fibers . . . 35

4 Discussion **36**
4.1 OpenFOAM . . . 36
4.1.1 Droplet position . . . 36
4.1.2 Droplet size . . . 36
4.1.3 Contact angle . . . 37
4.1.4 Surface tension . . . 38

4.1.5 Viscosity . . . 38
4.1.6 Density . . . 39
4.1.7 Impact velocity . . . 39
4.2 Water and ink-like liquid . . . 40
4.3 Technical discussion OpenFOAM . . . 41
4.4 HYDRUS . . . 42
4.4.1 Experiments . . . 42
4.4.2 Continuum-scale versus pore-scale modelling . . . 43
4.5 Future research . . . 45

5 Conclusion **46**

A OpenFOAM settings **48**
A.1 ControlDict . . . 48
A.2 fvSolution . . . 49
A.3 fvSchemes . . . 50

B OpenFOAM mesh files **51**
B.1 BlockMeshDict . . . 51
B.2 SnappyHexMeshDict . . . 52

C OpenFOAM boundary conditions **53**
C.1 Alpha.water . . . 53
C.2 Velocity . . . 54
C.3 Pressure (p_rgh) . . . 55

D HYDRUS settings **56**
D.1 Spatial discretization . . . 56
D.2 Time discretization and iteration criteria . . . 56

E Results OpenFOAM **57**
E.1 Infiltration plots . . . 57

Bibliography **59**

List of Figures

1.1 Continuous inkjet and drop on demand printing (obtained from Derby (2010)) . . . 1
1.2 FIBSEM images of coated paper. Obtained from Aslannejad et al. (2018a) 2
1.3 Ink spreading processes (Kettle et al., 2010) . . . 5

2.1 FIB-SEM images and reconstruction of the paper coating . . . 11
2.2 Meshing procedure with SnappyHexMesh . . . 14
2.3 Illustration of droplet on top of paper coating . . . 15
2.4 Conceptual model for HYDRUS . . . 18

3.1 Side view of final water droplet imprint. . . . 20
3.2 Infiltration of a water droplet into the paper coating. . . . 21
3.3 Results of the model validation. . . . 21
3.4 Comparison of the maximum spreading on the coating surface at two locations. . . . 22
3.5 Infiltration over time for the model validation simulations. . . . 23
3.6 Comparison of the final imprint of a water and ink droplet. . . . 23
3.7 Water content inside the coating layer for all simulations of the parameter study. . . . 25
3.8 Infiltration and spreading over time for different contact angles and surface tension . . . 26
3.9 Infiltration and spreading over time for a changing viscosity . . . 27
3.10 Infiltration and spreading over time for a changing density. . . . 28
3.11 Infiltration and spreading over time for droplets with and without an impact velocity . . . 29
3.12 Infiltration and spreading over time of a water and ink-like droplet . . 30
3.13 Flux through the constant head boundary . . . 32
3.14 Water content over time during infiltration of a large droplet (r = 20 µm) 33
3.15 Water content inside the coating during infiltration of a large droplet (r = 20 µm) . . . 33
3.16 Water content over time during infiltration of a small droplet (r = 3 µm) 34
3.17 Water content inside the coating during infiltration of a small droplet (r = 3 µm) . . . 34
3.18 Final imprint inside the coating and fibers . . . 35
3.19 Water content in horizontal and vertical direction inside the paper containing both a coating and fibrous layer. . . . 35

E.1 Relative water content of water, ink, surface tension and both contact angle simulations . . . 57
E.2 Relative water content of a sessile droplet (water) and a droplet with velocity of 5 m/s . . . 57
E.3 Relative water content of water, ink and both viscosity simulations . . 58
E.4 Relative water content of density simulations . . . 58

List of Tables

2.1 Properties of the coating layer and coated paper, derived from Aslannejad et al. (2017,2018a). 11
2.2 Results of FIB-SEM-CLSM imaging of droplet imprint 12
2.3 OpenFOAM boundary conditions 15
2.4 Parameters used in OpenFOAM simulations 17
2.5 Hydraulic properties of the coating and fibrous layer used in HYDRUS 18

3.1 Infiltration and spreading of all validation simulations. 22
3.2 All data regarding infiltration and spreading. 24
3.3 Results of the HYDRUS simulations 31

D.1 Mesh and geometry information 56
D.2 Settings regarding time discretization and iteration 56

List of Symbols

C	Courant number
d_0	droplet diameter before impact
g	gravitational acceleration
K	hydraulic conductivity
K_r	relative hydraulic conductivity
K_s	saturated hydraulic conductivity
l	length
l	empirical parameter in HYDRUS (Van Genuchten, 1980)
m	empirical parameter in HYDRUS (Van Genuchten, 1980)
n	empirical parameter in HYDRUS (Van Genuchten, 1980)
P	pressure
P_c	capillary pressure
Q	volumetric flow rate
r	capillary radius
S	saturation
t, T	time
U	velocity
V	volume
x	distance

α	volume fraction in OpenFOAM
α	empirical parameter in HYDRUS (Van Genuchten, 1980)
θ	contact angle
θ_r	residual water content
θ_s	saturated water content
θ_v	volumetric water content
μ	dynamic viscosity
ρ	density
σ	surface tension (generally used for interface between liquid and gas)
σ_{lg}	surface tension between liquid and gas
σ_{sg}	surface tension between solid and gas
σ_{sl}	surface tension between solid and liquid

1 Introduction

To print an image or text, several techniques have been developed, including offset printing, flexographic printing or inkjet printing. The last method is the most well-known and is also implemented in simple home office printers. During inkjet printing, small ink droplets are released ('jetted') from a nozzle above the paper surface to create an image. Nowadays, inkjet printing is also used as a technique to produce for example plastic electronics or solder droplets for the manufacturing of chips (Derby, 2010). Inkjet printing can be divided into two separate techniques of droplet formation. The first is continuous inkjet printing (CIJ), where the printer is creating droplets non-stop. Most of these droplets are flowing back into the printer, and only when the ink is actually needed to print an image, the droplets are ejected towards the paper. Another approach is drop-on-demand printing (DOD), where droplets are only created when needed (Kettle et al., 2010).

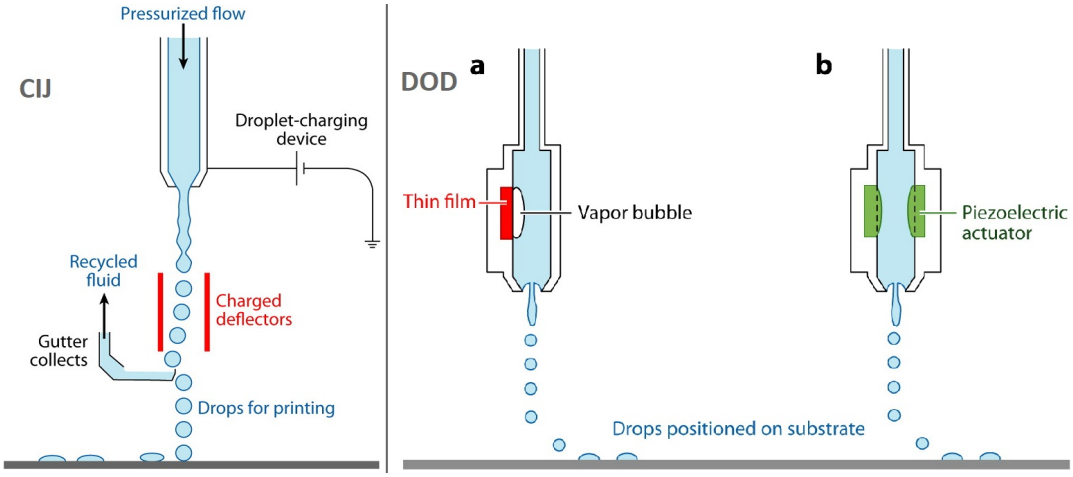

FIGURE 1.1: Left: Continuous inkjet (CIJ) printing. Right: two techniques of drop on demand printing (obtained from Derby (2010))

The paper that is used for printing can roughly be divided into uncoated and coated paper. Plain, uncoated paper consists of fibers, a porous material with a distinctive pore structure (Aslannejad and Hassanizadeh, 2017). In an earlier work (Aslannejad et al., 2018b), the infiltration of droplets on an uncoated paper is experimentally and numerically studied.

This study will mainly focus on coated paper. In this case, the fibrous layer is covered by a thin coating, consisting generally of kaolin or calcium carbonate. A cross-section of uncoated paper is shown in figure 1.2. The pore structure of the coating layer is very different from the pore structure of the fibrous material (Aslannejad et al., 2017; Aslannejad and Hassanizadeh, 2017; Aslannejad et al., 2018a).

For both CIJ or DOD, the nozzle, where droplets are created, is located at a certain distance above the paper. This means that a droplet will arrive at the paper surface with a certain velocity and will spread out over the paper surface and infiltrate into the paper. The fluid will eventually evaporate, after which only the pigment or dye

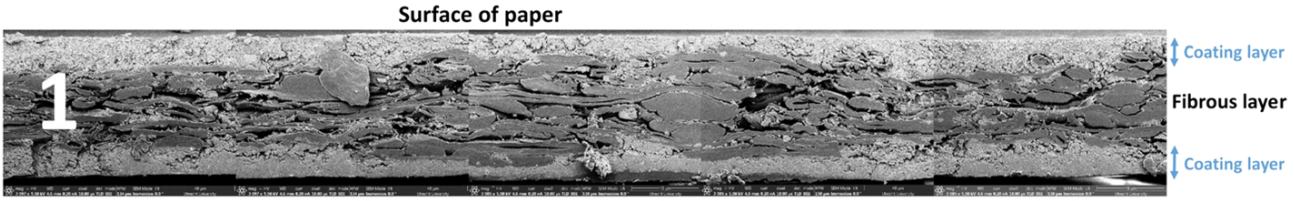

FIGURE 1.2: FIBSEM images of coated paper. Obtained from Aslannejad et al. (2018a)

is left in the paper (Kettle et al., 2010). Obviously, the aim with printing is to reach a high resolution image, with the least ink as possible. To achieve a high resolution, ideally the ink spreads out as little as possible and evaporate fast. If the droplets stay to long on the paper surface and spread too much, there is a possibility that the colours of several droplets that are printed close to each other could mix, which is called bleeding (Lamminmäki et al., 2011; Aslannejad et al., 2018a). Even mixing of drops with the same colour could have undesirable effects. These droplets could form one larger pool of liquid, which can cause a difference in dye density compared to other locations (Daniel and Berg, 2006). Also, droplets could be smeared when they stay at the paper surface.

Another important matter is to have a clear image at the paper surface, so the ink should stay in the top layer of the paper coating to fix the colouring part of the ink to the surface. This means that the infiltration should be slow, so the droplet has evaporated before the liquid has infiltrated too far. If the ink infiltrates too deep, more ink is needed to have the same clear colour at the surface. Besides, if the ink infiltrates too far into a coated paper, it may reach the fibrous layer below. The fibers itself are hydrophilic, so the ink will start to spread along the fibers ('wicking'). This will result in a spider-leg like ink distribution (Aslannejad et al., 2018a). In addition, when the solvent reaches the fibers, they could swell and cause deformation of the paper (Aslannejad and Hassanizadeh, 2017), which also decreases the print quality and can cause blockage of the printer. To satisfy these requirements, it is important to understand how an ink-like fluid will spread over and into a paper coating, and to know which factors influence this process.

1.1 Research objectives and thesis outline

In this thesis, the infiltration of small droplets into the coating layer of a paper will be studied numerically. A pore-scale model and a continuum-scale model will be developed and used to see which type of model is able to simulate more details of the droplet infiltration and is comparable with experimental results. With the use of the models, the influence of ink properties on the final imprint of an ink droplet can be shown. Therefore, the aim of this study is to find the best set of properties of the ink to achieve the highest print quality with the lowest volume of ink. The following research questions will be answered:

- Which are the optimal ink properties to achieve a desired ink imprint inside and on top of the coating layer of paper?
- Is it possible to simulate infiltration of small droplets into the thin coating layer of paper using a continuum-scale model?
- To what extent do a pore-scale model and a continuum-scale model yield similar results with regard to modelling of fluid flow within thin porous media?

This thesis will be arranged as follows: first, some background information will discussed, which consists of a review of relevant theory and literature on this topic. Chapter 2 contains the methods that are used, including the development of both models and an overview of the separate ink properties that will be studied. The results of both models will be presented separately in chapter 3 and discussed in chapter 4. In this chapter, the results of both models will be compared to each other and to data from earlier experiments. Moreover, the effect of changing ink properties on the imprint in a paper coating will be discussed. This chapter also contains a discussion of possible improvements to the models and possibilities for future research. Finally, in the last chapter, the main conclusions will be listed.

1.2 Background

1.2.1 Printing process

As explained in the introduction, inkjet printing is by definition a non-contact printing process, where the ink droplet is jetted towards the paper. Especially in DOD printing, the distance from the nozzle to the surface should be large enough (around 2-3 mm) for the droplet to form correctly (Derby, 2010).

When the droplet reaches the surface, the kinetic energy will cause the droplet to oscillate on the surface: it spreads out and bounces back several times before it reaches an equilibrium (Bahr et al., 2003; Kettle et al., 2010; Tan, 2017). According to Bahr et al. (2003) and Kettle et al. (2010), this oscillation will occur for aqueous ink droplets that has a diameter above 110 nm.

Lim et al. (2009) compared the oscillation of a high viscous fluid (ethylene glycol) and a low viscous fluid (water) after impact on a solid structure. The droplet diameter in their experiment was about 40 µm and the impact velocity was around 2 m/s. They concluded that a water droplet will both oscillate laterally as vertically. This means that during the first stages of droplet impact, both the contact area as the height of the droplet will change. Conversely, the ethylene glycol droplet did not show any lateral oscillations and only oscillated in height for one period. Lim et al. (2009) attributed this fact to the high viscous damping that occurs when a viscous fluid spreads out.

After a droplet is released onto the paper surface, several processes occur over different timescales until the ink is fully dried. Kettle et al. (2010) describe these processes over time, this is shown in figure 1.3. The first process is the spreading of the droplet over the surface, which quickly also competes with infiltration due to capillary forces. As seen in figure 1.3, the penetration starts 0.1 ms after the droplet arrives on the paper surface. Soon after starting the imbibition into the paper, the ink components separate, followed by adsorption onto the coating, diffusion of several ink components, polymerization and drying. Ideally, the color of the ink (in the form of pigments or dye), is deposited on the paper surface, while the other ink components (like the solvent) move further into the porous structure (Kettle et al., 2010). This study will focus on the first two phenomena: the spreading and penetration of an ink-like fluid, without separation or other component-specific processes.

The type of ink that will be considered in this study will be a general water-based (aqueous) ink, which will be called an ink-like liquid. The components can generally be divided into 60% water, 30% humectant (for example ethylene glycol), 2-5% surfactants and 2-5 % (by weight) dye or pigment (Lee et al., 2002). Surfactants are important, as they increase the speed of droplet infiltration. They alter the surface tension between the fluid and the solid surface (Daniel and Berg, 2006).

1.2.2 Capillary pressure and viscous drag

When a droplet is placed on a porous medium, it will spread out over the surface, but also infiltrate into the pores. The processes that influence these spreading mechanisms need to be known to describe the final imprint of a droplet in and on the paper surface.

The infiltration of a water droplet into the paper is an example of two-phase flow, with a wetting fluid (water or ink) and a non-wetting fluid (air). When a droplet is placed on a non-porous surface, the angle of the droplet and the solid surface

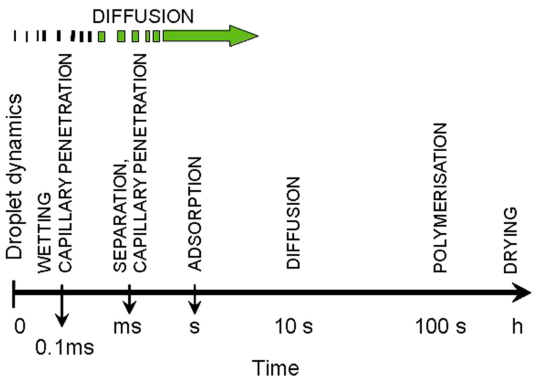

FIGURE 1.3: The different processes that occur after the release of an ink droplet over time (Kettle et al., 2010)

is called the intrinsic contact angle. A fluid is considered fully wetting when the contact angle is 0° and partially wetting between 0 - 90°.

Because the wetting fluid is more attracted to the solid phase, capillary rise occurs. With capillary rise, the wetting fluid makes contact with the tube under the same contact angle. This forms an interface between the wetting and non-wetting fluid in the shape of a meniscus over which the pressure drops. This pressure is described with the Young-Laplace equation (Kettle et al., 2010):

$$P_c = P_{nw} - P_w = \frac{2\sigma_{lg}\cos\theta}{r} \tag{1.1}$$

The contact angle (θ) of equation 1.1 is defined by the Young-Dupré equation (Kettle et al., 2010; Daniel and Berg, 2006):

$$\cos\theta = \frac{\sigma_{sg} - \sigma_{sl}}{\sigma_{lg}} \tag{1.2}$$

Where σ_{sg}, σ_{sl} and σ_{lg} are the surface tensions of the interfaces between the solid-gas, solid-liquid and liquid-gas phases.

It should be noted that when a droplet is placed on a porous structure, the visible contact angle at the surface can be different from the intrinsic (Young) contact angle as described in equation 1.2. This contact angle can change due to different factors, like evaporation or infiltration into the porous medium. Also, during the initial spreading of a droplet on the surface, the contact angle will differ from the intrinsic contact angle. Often, a dynamic contact angle is used in modelling, that changes from an advancing contact angle to an receding contact angle. The advancing contact angle is occurring during the initial spreading of a droplet, while the receding contact angle is associated with a shrinkage of the droplet at the surface due to evaporation or infiltration. The advancing contact angle is larger compared to the receding contact angle (Gambaryan-Roisman, 2014; Brutin and Starov, 2018). An indication of the difference between the advancing and receding contact angle can be found in a paper by Tan (2017). They measured that these are respectively 85°and 21°for an aqueous ink on paper sample (the paper properties are undefined).

Inside a capillary or a porous medium, the Laplace pressure (eq. 1.1) results in a force that causes the liquid to move into the structure. This force is counteracted by a viscous drag force, that can be described with Poiseuille's Law:

$$Q = \frac{dV}{dt} = \frac{\pi r^4}{8\mu l} P_c \tag{1.3}$$

This formula describes that the pressure within a tube is driven by the pressure difference (capillary pressure) and is counteracted by resistance. This resistance, the viscous drag, occurs at the sides of the tube. It results in a higher velocity in the middle of the tube compared to the flow velocity close to the sides.

1.2.3 Fluid infiltration

A simple model to describe the height of the capillary rise is described by Lucas and Washburn (Washburn, 1921). They combined Poiseuille equation (drag force) and the Young-Laplace equation (wetting force) and derived the following equation (see equation 1.4) for the distance travelled in a horizontal capillary tube (Kettle et al., 2010; Schoelkopf et al., 2000; Ridgway and Gane, 2002).

$$x(t) = \sqrt{\frac{r\sigma_{l_g} t \cos\theta}{2\mu}} \tag{1.4}$$

This equation is often used to describe the infiltration into a porous medium, because of the simplicity of the model. The distance $x(t)$, which is the penetration depth, should increase with increasing pore radius. Many studies found that infiltration into a porous network is different from the Lucas-Washburn equation (eq. 1.4). For example, studies by Schoelkopf et al. (2000) and Ridgway and Gane (2002) describe that the smallest pores will fill faster than the larger pores, which contradicts equation 1.4. This preferential filling of finer pores can result in some preferred pathways, this can cause some pores to not fill at all during imbibition if there is a small amount of fluid present (Schoelkopf et al., 2000).

To explain the faster filling of the finer pores, some studies (Schoelkopf et al., 2000; Liu et al., 2017; Ridgway et al., 2002; Ridgway and Gane, 2002) argue that the effect of inertia of the fluid, influenced by the fluid density, should be considered. They discuss the effect of inertial delay, in which acceleration by capillary forces is inhibited by the inertia of the fluid. To incorporate the effect of inertia, the model of Bosanquet (Bosanquet, 1923) is often used (Schoelkopf et al., 2000; Ridgway et al., 2002; Liu et al., 2017). The travelled distance in a capillary according to the model of Bosanquet will be described as follows (Bosanquet, 1923):

$$x(t) = t\sqrt{\frac{2\sigma\cos\theta}{\rho r}} \tag{1.5}$$

This model is based on the assumption that flow is independent on viscosity. This means that there is no drag at the sides of a pore and therefore flows with a flat front inside a capillary. This is opposite from flow according to Poiseuille's law, where the flow front in parabolic, because the flow is slowed down close to the sides of the pore due to viscous drag. Note that the height in a capillary according to the Lucas-Washburn equation (eq. 1.4) is proportional to the radius, while the height according to Bosanquet (eq. 1.5) is inversely proportional to the radius.

For infiltration into a porous medium, it was found that a combination of the models of Lucas-Washburn and Bosanquet yields better results. At the beginning of droplet infiltration the flow is described with the model of Bosanquet, but after some time it will switch to flow as described by Lucas-Washburn. The transition

will be influenced by pore radius and viscosity and density (Schoelkopf et al., 2000; Ridgway and Gane, 2002). Experimental data of Liu et al. (2017) also show this transition between the models of Lucas-Washburn and Bosanquet on coated paper. They also show that the presence of fibers, especially in uncoated paper, causes a deviation from this expected behaviour.

The fact that a combination of both models is often used, indicates that both viscous drag (which is described in Lucas-Washburn) and the effect of inertia (Bosanquet) is important. This interplay between viscous drag and inertial retardation will result in an optimal pore size for fluids to infiltrate (Ridgway et al., 2002). More specifically, viscous drag will have a large effect in the finest pores, while inertial effects will slow down the flow in the large pores. Ridgway et al. (2002) studied this effect for an optimal 'aspect ratio' which is the ratio of throat length (l) to throat radius (r). They concluded that a preferred pathway will form through the throats with this optimal l/r value. This optimal pore size will differ for fluids with a different viscosity and density (Ridgway and Gane, 2002). The pore size distribution will influence the infiltration rate, but can also change the final infiltration depth (Ridgway et al., 2002; Ridgway and Gane, 2002).

The Lucas-Washburn and Bosanquet models describe the flow through a single capillary tube. Studies that apply these equations, often assume that a porous medium can be described as a bundle of capillary tubes. This oversimplifies the real pore structure, as it does not incorporate important features like pore connectivity or pore shape. The importance of these kind of features is shown in the study of Rahimi et al. (2016), who compared three models with the same pore size distribution, but a different pore structure. They showed that the imprint of the fluid in every structure was different. This means that the models of Lucas-Washburn and Bosanquet are too simple to describe the complex infiltration in a porous medium.

Moreover, when regarding droplet infiltration, one should also incorporate spreading over the surface of the porous medium. The surface spreading and infiltration will occur simultaneously (Daniel and Berg, 2006; Bonn et al., 2009; Gambaryan-Roisman, 2014), although some studies assume that a droplet first spreads on the surface before it infiltrates the porous structure (Starov et al., 2002; Tan, 2017). Several different approaches have been used to model droplet infiltration. An extensive review of all these models can be found in Gambaryan-Roisman (2014), some of them are explained in the next section.

1.2.4 Previous studies

One way to model simulataneous spreading and infiltration is described by Davis and Hocking (1999,2000), who applied lubrication theory. They developed a two-dimensional model where the porous structure is assumed to consist of vertical tubes with equal width. This model contains a description of fluid transport on the surface of the structure, while also solving the droplet volume loss by infiltration into the porous structure, governed by capillary action. Desie et al. (2004) compared this model with experiments of the infiltration of aqueous inks containing dye or pigments. They concluded that only dye based ink infiltration could be described with the Davis-Hocking model. The pigments in the other ink were deposited on the substrate and blocked the pores from imbibing the fluid, which resulted in flow that deviates from the Davis-Hocking model.

Starov et al. (2002) developed a hydrodynamic model that solves Darcy's law for the flow inside the porous medium to describe the spreading and infiltration of a droplet that is much larger compared to the thickness of the porous medium. By

using this criterion, they assumed that the porous medium underneath the droplet is directly saturated. They assumed that the spreading of the droplet on the paper surface occurred much faster compared to the fluid movement inside the porous structure. Consequently, they could model the two processes independently.

In hydrodynamic theory, it is assumed that initially, when the droplet impact drives the movement, the diameter of the contact surface of the droplet can be scaled as $D \sim t^{1/2}$. After the effect of the droplet momentum during the inertial stage diminishes, capillary force drives the spreading over the surface. During this stage, the diameter scales as $D \sim t^{1/10}$, which is often referred to as Tanner's law (Tanner, 1979; Daniel and Berg, 2006; Koivula et al., 2012)

The model of Alleborn and Raszillier (2004) also applies lubrication theory and uses the Navier-Stokes equations and the continuity equation to describe the flow on top of the paper surface and applies Darcy's flow inside of the porous medium. The porous medium is incorporated by means of the porosity, permeability and a 'suction number', which includes the capillary pressure and surface tension.

Daniel and Berg (2006) used the energy balance of the droplet to develop a model of spreading and infiltration of a droplet on and into a porous surface. With this model, they were able to predict the droplet radius and volume on a porous surface and a fluid profile inside the porous structure. They studied the effect of surfactants in the fluid, which are substances that lower the surface tension of a fluid. Their model works best for fully wetting fluids with a high concentration of surfactants and they concluded that their energy-based model was unfit to describe the spreading of a non-wetting fluid.

In many of the models described above, flow inside of the porous medium is described with the use of Darcy's law (Davis and Hocking, 1999; Starov et al., 2002; Alleborn and Raszillier, 2004; Gambaryan-Roisman, 2014). This means that the models all assume a sharp interface between the saturated and dry areas. In reality, the wetting front is not sharp and consists of pores that are partly filled or empty next to pores that are saturated (Schoelkopf et al., 2000; Gambaryan-Roisman, 2014). Yin et al. (2018) found that the saturation front becomes sharper when the droplet size becomes smaller, but that even for 2 pL droplets the interface is not perfectly sharp. They suggest the use of Richards equation instead of Darcy's law. The studies that will be discussed next have implemented other approaches to model droplet behaviour.

Markicevic and Navaz (2010) used numerical multiphase modelling in a regular capillary network to describe droplet infiltration. This means that they also incorporate evaporation and the occurrence of gas clusters within the fluid fraction. They distinguished between primary spread, which is the movement of the liquid through the porous medium, while there is still fluid present on the surface. Secondary spread takes place after the droplet is fully imbibed by the porous medium, but the fluid is still moving inside the porous medium. Evaporation starts when the droplet is imbibed into the porous structure. They did not take into account the spreading on top of the porous structure, so they used a fixed droplet base at the surface.

Another pore network is used by Rahimi et al. (2016). They generated a two-dimensional network to study the whole process from droplet deposition to evaporation. First, the droplet infiltrates the network and when the liquid at the surface is depleted, the evaporation stage starts. They studied the effect of fluids with varying viscosities and the effect of different pore structures. Gravity and inertia are not taken into account. They found that a very low viscosity will significantly increase the infiltration rate, whereas a fluid with a very high viscosity ('infinite viscosity'),

barely infiltrates a porous structure. Furthermore, they argued that the viscous drag of a high viscous liquid will increase during penetration of the liquid, because the fluid flows through an increasing number of pores. This also means that the rate of spreading through the porous structure will decrease.

Recently, Yin et al. (2018) have developed a pore-network model based on the hydraulic properties of a real paper coating. These properties are based on the same sample of the paper coating that will be used in this study. They only modelled movement inside the coating layer, hence the contact area of the droplet on the paper surface is fixed. They found that a lower surface tension, higher viscosity or higher contact angle will decrease the infiltration rate.

Tan (2017) developed a model of imbibition and spreading of an impacting, picoliter-sized droplet on thin porous substrates. They assumed that the timescales for surface spreading, infiltration and evaporation were significantly different and therefore they decoupled these processes in their model. The spreading of the droplet on the surface is modelled by using computational fluid dynamics (CFD), that solve the Navier Stokes equations, and implementing the volume of fluid method. Inside the porous medium, the volume averaging method is implemented. This means that an average velocity and pressure inside a representative elementary volume (REV) is used to use the Navier-Stokes equations inside the porous medium. They found that an increase in impact velocity causes the droplet to spread out further. Moreover, they concluded that this lateral spreading is reduced when the viscosity becomes higher, because the viscous force decreases the momentum of the droplet.

Recently, Fu et al. (2019) also used CFD modelling combined with the volume of fluid method to study the spreading and infiltration of droplets on porous substrates. They argue that spreading and infiltration could occur simultaneously, hence these are not decoupled as in the model of Tan (2017). The porous medium is based on randomly packed spheres, by using a standard particle size and permeability. They found that both the spreading and infiltration of a droplet will be hindered when the contact angle increases.

1.2.5 Pore-scale versus continuum-scale modelling

In this study, two type of models will be used: a direct pore-scale and a continuum-scale model. With direct pore-scale modelling, the computational domain will be an exact representation of the porous medium, which means that there is no need for any approximations to describe the pore structure. This modelling will be carried out by using the software OpenFOAM (The OpenFOAM Foundation, 2018). A detailed description and the equations that will be used, can be found in chapter 2.

The continuum-scale is also called the Darcy scale, which is the scale at which Darcy's law is generally valid to use. Continuum-scale models use average properties to describe the porous medium. These average properties are defined to be valid at a certain minimum volume that is called the representative elementary volume (REV) (Szymkiewicz, 2013). A REV should contain a large number of pores and should be much smaller than the full size of the domain that is modelled. In the case of a paper coating, this is impossible to achieve since the coating thickness is very low (about 12 µm) (Aslannejad et al., 2018a). Still, a continuum-scale model may be useful, especially because it will be much easier to implement compared to a pore-scale model and the computational demand will be lower.

The models of Lucas-Washburn or Bousanquet both solve Darcy's law and thus are continuum-scale models. As previously discussed, there are many shortcomings in using these models. One of the issues is the occurrence of a wetting front inside

the porous medium that is not sharp (Gambaryan-Roisman, 2014). To improve this, Richards equations could be used, which also accounts for saturation (Yin et al., 2018). In this study, the software HYDRUS-2D (Šimůnek et al., 2006) will be used for the continuum-scale modelling.

In this study, we will check whether a continuum-model is able to produce valid results and is able to describe the infiltration of small scale droplets into a paper coating.

1.2.6 Ink properties

Several dimensionless numbers are used to describe the wetting process. The first is the Bond number, that describes whether gravity will play a significant role in the motion of a falling droplet (Kettle et al., 2010; Tan, 2017). It is calculated as follows:

$$Bo = \frac{\rho g r^2}{\sigma} \tag{1.6}$$

A Bond number below 1 denotes that that gravity does not play a big role and that surface tension is the dominating process in droplet motion (Kettle et al., 2010). The droplet size considered in inkjet printing is generally so small that the Bond number is always below 1, so the influence of gravity in this study will be negligible.

Another useful number is the Weber number, which is important when considering droplets that arrive with a certain velocity at the paper surface (Kettle et al., 2010; Koivula et al., 2012; Tan, 2017):

$$We = \frac{\rho d_0 U^2}{\sigma} \tag{1.7}$$

This number shows whether the liquid movement is driven by the inertia due to a falling droplet or the surface tension (Koivula et al., 2012). Moreover, it will denote whether splashing is expected to occur when a droplet hits the surface. This will generally occur when the Weber number is above 250 (Yarin, 2006; Tan, 2017).

The last important number is the Ohnesorge number, which shows the forces that slow down the liquid movement. It is the ratio between viscous force to inertia and surface tension (Koivula et al., 2012; Tan, 2017):

$$Oh = \frac{\mu}{\sqrt{\rho d_0 \sigma}} \tag{1.8}$$

To achieve the best results with droplet formation at the nozzle, the Ohnesorge number should be between 0.1 and 1 (Derby, 2010).

These dimensionless numbers and the equations in the previous sections show that there are several fluid properties that will influence the rate and distance of liquid infiltration inside an porous medium. Therefore, the effect of viscosity, density, surface tension, contact angle, impact velocity and droplet volume will be studied in this thesis.

2 Methods

This chapter discusses the methods that will be used to answer the research questions. First, yet unpublished experimental data on the infiltration of droplets into the paper coating will be shortly reviewed, as well as the hydraulic properties of the coating layer (Aslannejad et al., 2017). This data will be used to validate the model output. Next, the development of the pore-scale model will be described. In the section 'parameter study', the fluid properties are listed that will be tested with the use of the pore-scale model. Lastly, the continuum-scale model will be discussed.

2.1 Experimental data

A previous study (Aslannejad et al., 2017) has been carried out to determine the pore structure and properties of a paper coating layer. These properties are listed in table 2.1. The REV is determined to be 60 μm^3 Aslannejad et al. (2017). With the use of scanning electron microscopy combined with focused ion beam (FIB-SEM) the pore structure could be reconstructed. This technique yields images of thin layers of the paper sample, which were used to create a 3D image of the sample (see figure 2.1) (Aslannejad et al., 2017). The final domain size that can be used in the numerical simulations is 6.1 x 2.9 x 4.4 µm.

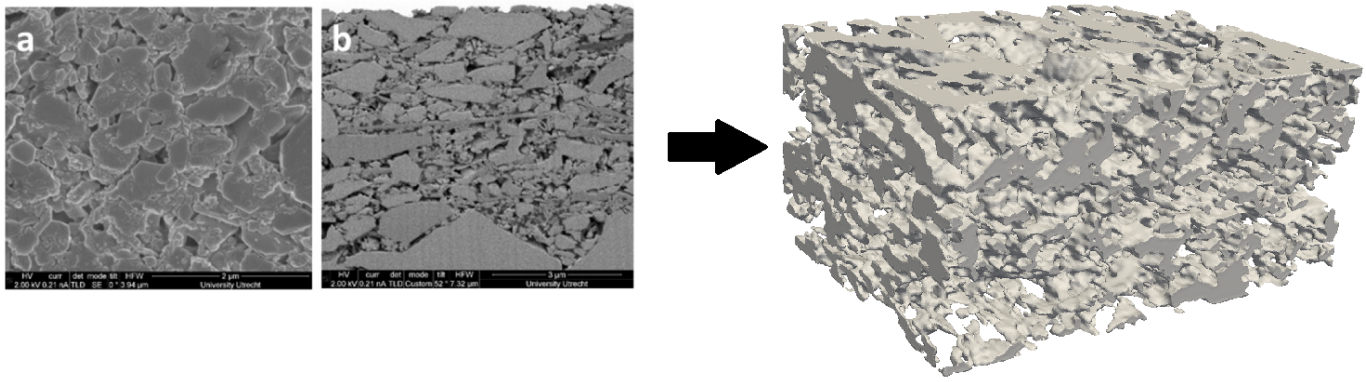

FIGURE 2.1: Left: FIB-SEM images of surface (a) and side (b) of paper coating (Aslannejad et al., 2017). Right: reconstruction of the paper coating (6.1 x 2.9 x 4.4 μm)

TABLE 2.1: Properties of the coating layer and coated paper, derived from Aslannejad et al. (2017,2018a). The paper was Sappi Magno Gloss (see www.sappi.com/magno-gloss).

	Thickness (μm)	**Porosity** (%)	**Mean pore size** (nm)	**Permeability** ($mDarcy$)	**Chemistry** (%)			**Grammage** (g/m^2)
					$CaCO_3$	**Talc**	**Binder**	
Coating layer	12.8	34	180	0.1	88	2.2	9.8	-
Coated paper	85	-	-	-	-	-	-	115

An experiment has been carried out to examine the spreading of the ink in the paper coating (yet unpublished). In this experiment, ink droplets were placed on the paper coating. The droplet volume is not known exactly, but is about 30 pL. This size is based on the cartridge type of the printer that was used. After the infiltration and evaporation of the droplet has occurred, the spreading on the surface and the penetration depth was measured. This was done by looking at the SEM images and also by obtaining images with the use of Confocal Laser Scanning Microscopy (CLSM). This process is further explained in the paper of Aslannejad et al. (2017). The results of the imaging of three droplets is listed in table 2.2, which is described under 'normal stains'. Satellite stains are created due to splashing of the falling droplet and have a much smaller, but undefined, volume.

TABLE 2.2: Results of FIB-SEM-CLSM imaging of droplet imprint.

	Normal stains			**Satellite stains**	
Diameter at surface (µm)	30	45	50	10	6
Penetration depth (µm)	5.5	10	11	3	2

2.2 Pore-scale model

To simulate the imbibition of ink into paper on the pore-scale, the open-source software OpenFOAM (The OpenFOAM Foundation, 2018) will be used to develop a model.

2.2.1 Equations

OpenFOAM is computational fluid dynamics (CFD) software that solves the Navier-Stokes equations. These comprise a continuity equation (equation 2.1), which describes the conservation of mass, and an equation for the conservation of momentum (equation 2.2). Because it could be assumed that the fluid is incompressible, the continuity equation is:

$$\nabla \cdot U = 0 \tag{2.1}$$

The momentum conservation equation could be written as (Fathi et al., 2017):

$$\frac{\delta(\rho U)}{\delta t} + \nabla \cdot (\rho U U) = \rho g + \nabla \cdot \mu(\nabla U) - \nabla P - F_\sigma \tag{2.2}$$

The left hand side of the equation describe the inertial forces that act upon the fluid. On the right hand side, the first term describes the force by gravity, the second term the viscous forces, the third describes the pressure forces, and the last term the surface tension force (Fathi et al., 2017).

The interFOAM solver of OpenFOAM will be used, which can be used for cases with two incompressible, isothermal, immiscible fluids (The OpenFOAM Foundation, 2018). This solver applies the volume of fluid method (VOF), which means that the whole pore space can be modelled as if it contains one fluid, but the properties of this fluid will vary spatially. For this, a fluid fraction (denoted by α) will be assigned to every cell, where $\alpha = 1$ describes a cell that is fully filled with the wetting fluid and $\alpha = 0$ describes a cell that is fully filled with the non-wetting fluid. A value between 0 and 1 is assigned to cells that contain the interface between the wetting and

non-wetting fluid. The fluid properties in every cell are also calculated with the use of α. For example the density will be calculated as follows (Deshpande et al., 2012):

$$\rho = \alpha\rho_w + (1 - \alpha)\rho_{nw} \tag{2.3}$$

Where μ is the viscosity used in the grid cell and μ_w and μ_{nw} are the dynamic viscosities of the wetting and non-wetting fluids, respectively.

The movement of the interface of the wetting and non-wetting fluid can be described as follows (Deshpande et al., 2012):

$$\frac{\delta\alpha}{\delta t} + \nabla \cdot (\alpha U) = 0 \tag{2.4}$$

This equation is usually modified to reduce numerical diffusion. Numerical diffusion should always be avoided, since it could cause the interface between the wetting and non-wetting fluid to become smeared out over many cells, i.e. there are many cells where α is between 0 and 1 (Deshpande et al., 2012; Fathi et al., 2017).

2.2.2 OpenFOAM structure

The following list contains all settings that are needed for an OpenFOAM simulation. The exact settings can be found in appendices A, B and C.

- Numerical settings (see appendix A):
  - Discretization schemes (fvSchemes)
  - Solver and algorithm settings (fvSolution)
  - Time and data handling (controlDict)
- Mesh (see appendix B)
- Initial and boundary conditions (see appendix C):
  - Velocity
  - Pressure
  - α
- Constants:
  - Kinematic viscosity
  - Density
  - Surface tension between wetting and non-wetting fluid
  - Gravity

The next sections will describe the important settings in more detail.

2.2.3 Meshing

The 3D image of the paper coating (fig. 2.1) is used as input to create a mesh. This is done by using the dictionaries *blockMesh* and *snappyHexMesh* of OpenFOAM and shown in figure 2.2. First a 3D regular grid that consists of hexahedral cells is created with the use of the *blockMesh* dictionary (also see appendix B.1). This grid is the base mesh and consists of cells that are 60 x 60 x 60 nm (see left image in fig. 2.2).

SnappyHexMesh first removes all cells of the base mesh that are located in the solid part (the grains) of the coating. Moreover, the cells in the pore space that are situated close to the solid grains get refined. This means that a cell will be split into 8 smaller cells of about 30 x 30 x 30 nm. The result is a mesh that represents

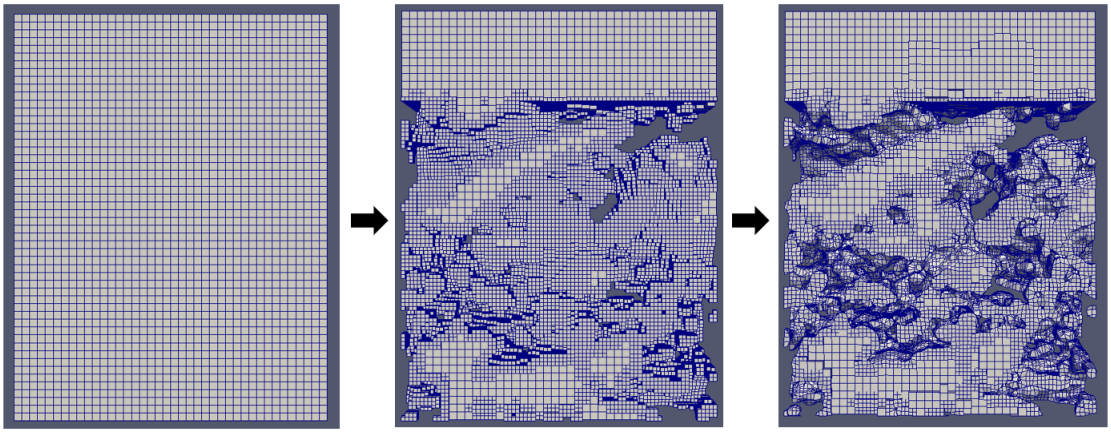

FIGURE 2.2: Meshing procedure with SnappyHexMesh. Left: blockmesh, middle: castellated mesh, right: snapped mesh.

the pore space, but without any smooth surfaces (see middle image in fig. 2.2). In the last stage, the cells that are located on the edges of a pore are snapped to get a smoother image of the pore space (see last image of fig. 2.2). The exact settings in SnappyHexMeshDict can be found in Appendix B.2.

The resulting domain is too small to use in the simulations, although the full size of the FIB-SEM images is used. To increase the domain size, the 3D image is mirrored and duplicated in every direction with the use of Blender (The Blender Documentation Team, 2019). This yields a domain that is eight times larger than the original domain, which is suitable for the infiltration of the largest droplet (r = 3 µ). For the simulations with a smaller droplet size, the duplicated domain is cropped again to obtain the smallest possible domain size.

Besides, two sides are declared as 'symmetryPlane' within *blockMeshDict* over which the solution will be mirrored. This way, the computational domain can be assumed to comprise one quarter of the full domain, which decreases the computational time to run a simulation, while still maintaining a relatively large droplet size. Subsequently, only a quarter of a sphere will be used in the simulations. An earlier study has shown that, by using a pore-network model with the same properties as the paper coating here, a quarter droplet is good enough to capture the main features of the droplet movement through the coating (Yin et al., 2018).

2.2.4 Initial conditions

After the mesh is created, it can be used for the actual flow simulation. The domain should be initialized for alpha, pressure and velocity. The pressure in the whole domain is assumed to be at atmospheric pressure and is therefore set at 0. The initial velocity in the whole domain is also 0 m/s.

To create a droplet of water that can infiltrate the porous medium, the utility 'setFields' of OpenFOAM is used. A quarter of a sphere with an alpha value of 1 at the initial location of the droplet is intersecting with the symmetryPlanes. This is illustrated in figure 2.3.

The droplet radius is 2 µm for most simulations. This size is smaller than the droplet size used in the experiments and also smaller than the droplet size that is used in inkjet printing (Kettle et al., 2010; Derby, 2010). However, this small size is necessary to decrease the computational time that is needed to run one case.

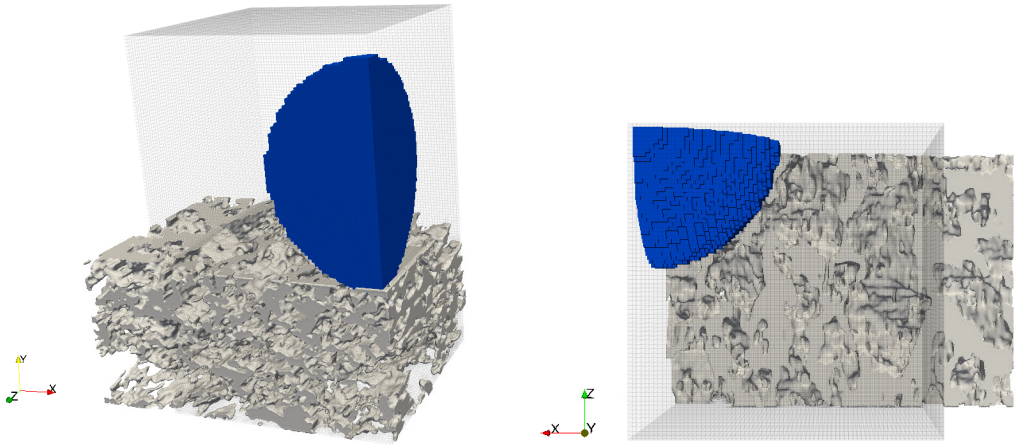

(A) Sideview (B) Topview

FIGURE 2.3: Illustration of droplet on top of paper coating. The grid cube is the mesh that will be used.

2.2.5 Boundary conditions

The exact settings of the boundary conditions for alpha, velocity and pressure can be found in Appendix C. The conditions are set for all sides of the computational domain (including the top and bottom) and at the coating grains itself. The conditions at the bottom and sides of the mesh are equal; at the coating and at the top of the mesh the boundary conditions are different. An overview of the boundary conditions can be seen in table 2.3. The sides that are symmetry planes have no specified boundary conditions, except for the symmetry condition.

TABLE 2.3: Boundary conditions. The values in brackets indicate the value that is set for this condition

	Alpha	**Velocity**	**Pressure**
Top	`zeroGradient`	`fixedValue`	`fixedFluxPressure`
Sides	`inletOutlet`	`pressureInlet-OutletVelocity`	`totalPressure`
Coating	`constantAlpha-ContactAngle`	`fixedValue`	`fixedFluxPressure`

These boundary conditions specify that flow could occur at the sides of the domain, except for the top. Also, the boundary conditions at the grains are no-slip with a fixed contact angle.

2.2.6 Time settings

Every simulation will run until the droplet is fully inside the coating layer. The results will be written with an interval of 5e-7 seconds. However, the timestep for the calculations will be adjusted by the model, by using the setting *adjustTimeStep*. It uses the maximum Courant number to check whether the time step should be decreased or could increase. This number is used to satisfy the Courant-Friedrichs-Lewy condition that makes sure that the time steps are small enough to make the

solution converge. The Courant number is calculated as follows:

$$C = \frac{U\Delta t}{\Delta x} \leq C_{max} \tag{2.5}$$

The value for C_{max} is specified in the *controlDict* file. Since the value of Δx is constant for a certain cell and the value of U is known, only Δt could be changed to keep the Courant number low. Generally, the Courant number has to stay below 1, but OpenFOAM sometimes overshoots the maximum value. Therefore, C_{max} is set at 0.7 to prevent C to become higher than 1.

The simulations are run in parallel on 84 processors on a cluster. Still, the computational time for one simulation is around 100 hours.

2.2.7 Model validation

All simulations will be carried out with a droplet (r = 2 µm) on a fixed location in the coating. To see whether the outcome of the OpenFOAM model is independent on the pore structure at that location, the infiltration simulation is also carried out with a quarter of a water droplet of the same size at another corner of the domain.

Moreover, one simulation will be carried out with a droplet radius of 3 µm, to see the effect of droplet size. This simulation could also be used to compare the results to the experiments. One of the satellite droplets that was formed during the experiments had a spreading radius of 3 µm (see table 2.2). If we assume that this radius is equal to the droplet radius before impact, the imprint of this satellite can be compared to the OpenFOAM results. This assumption is valid since the surface of coating layer is designed to confine the droplet shape and prevent spreading over the paper surface.

2.2.8 Parameter study

With the OpenFOAM model, a parameter study will be carried out to study the effect of different ink properties: contact angle, viscosity, density and surface tension. Besides studying the effect of the ink properties separately, the infiltration of water and an aqueous ink will be compared. Moreover, the effect of the velocity of a droplet when it impacts the coating will be studied. The values that are used in the various runs are denoted in table 2.4.

The values for water and an ink-like fluid are based on values used in Aslannejad et al. (2018b) and Kettle et al. (2010). The contact angle for a calcite surface is assumed to be 45° based on the papers by Järnström et al. (2010) and Yin et al. (2018). It is assumed that an aqueous ink contains between 30% and 60% glycerol. These glycerol percentages are used to derive the values for the simulations with a respectively low and high viscosity and density (Cheng, 2008; Volk and Kähler, 2018). To check the effect of a different wettability of the fluid, the contact angle is changed to 1° and 90°.

According to Derby (2010), the distance between the nozzle and the paper should be at least 2 - 3 mm. However, this would result in a computational domain that is too large. Therefore, the initial condition of the impact velocity simulation is equal to the other simulations, i.e. the droplet starts as a sphere that contacts the paper surface. However, within this sphere a velocity in the y-direction is specified. The estimates in previous studies of the inkjet droplet velocity before impact range generally between 2 m/s (Lim et al., 2009) to 10 m/s (Desie et al., 2004; Daniel and Berg, 2006). In this study, we will use a velocity of 5 m/s.

TABLE 2.4: Parameters used in OpenFOAM simulations

Simulation run	**Kinematic Viscosity** (m^2/s)	**Density** (kg/m^3)	**Surface tension** (kg/s^2)	**Contact angle (°)**	**Impact velocity** (m/s)
Water	1e-6	1000	0.072	45	0
Ink-like fluid	2e-6	1050	0.03571	45	0
High contact angle	1e-6	1000	0.072	90	0
Low contact angle	1e-6	1000	0.072	1	0
Viscosity (30% glycerol)	2.6739e-6	1000	0.072	45	0
Viscosity (60% glycerol)	13.117e-6	1000	0.072	45	0
Density (30% glycerol)	1e-6	1085.6	0.072	45	0
Density (60% glycerol)	1e-6	1167.0	0.072	45	0
Low surface tension	1e-6	1000	0.03571	45	0
Impact velocity	1e-6	1000	0.072	45	5

2.3 Continuum-scale model

Beside the pore-scale modelling, the infiltration of a water droplet into the coating layer of paper will also be studied with the use of a continuum-scale model. This modelling will be carried out with the software HYDRUS-2D (version 2.05) (Šimůnek et al., 2006).

2.3.1 Equations

HYDRUS solves a solution for the Richards equation (Šimůnek et al., 2006), which describes the flow in a porous medium by calculating the change in saturation. For one-dimension, it can be written as follows:

$$\frac{\delta\theta}{\delta t} = \frac{\delta}{\delta z}\left[K(\theta)\left(\frac{\delta h}{\delta z} + 1\right)\right] \tag{2.6}$$

Where $K(\theta)$ = unsaturated hydraulic conductivity [m/d], which can be written as follows:

$$K(\theta) = K_r(h)K_s \tag{2.7}$$

Besides, the hydraulic model by van Genuchten and Mualem is used (Mualem, 1976; Van Genuchten, 1980). The hydraulic properties of the coating are incorporated using the following equations:

$$\theta(h) = \theta_r + \frac{\theta_s - \theta_r}{(1 + |\alpha h|^n)^m} \tag{2.8}$$

Where $h < 0$. When $h \geq 0$ the equation reduces to $\theta(h) = \theta_s$

$$K_r(h) = K_s S^l [1 - (1 - S^{1/m})^m]^2 \tag{2.9}$$

$$S = \frac{\theta - \theta_r}{\theta_s - \theta_r} \tag{2.10}$$

In these equations, α, l, n and m are empirical parameters, where $m = 1 - 1/n$. α is the inverse of the air entry pressure, l is a parameter that describes pore connectivity and n is an index for the pore size distribution.

2.3.2 HYDRUS

In this section, the most important settings for the HYDRUS model will be discussed. All other settings can be found in appendix D.

2.3.3 Geometry and mesh

The conceptual model for the HYDRUS simulations is shown in figure 2.4. The problem is approached by using an axisymmetrical 2D domain, which is a quasi-3D system and is generally used for radial flow problems. The black cylinder in figure 2.4 is the part of the paper that will be modelled, the red square indicates the computational domain. The position of a droplet is approached by a fixed wetted surface area at the top of the domain, which is the blue circle at the top of the cylinder. The gray area indicates the interface between the coating and the fibrous layer. The computational domain (red square) is constructed with a finite element mesh, where the cells at the paper surface are small and are gradually increasing in size towards the bottom. This is needed to yield a converging solution.

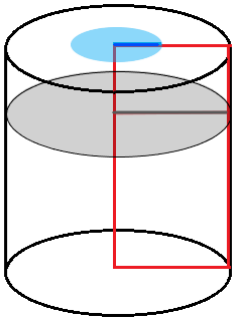

FIGURE 2.4: Conceptual model for HYDRUS

Three different cases will be studied, all cases have a slightly different geometry. The first case comprises both the coating and the fibrous layer and has an infiltrating droplet of a radius of 20 µm. In the other two cases only the coating is present, but the infiltrating droplet has a radius of 20 µm or 3 µm. This way, the HYDRUS results can be compared with the experimental data and the results of the OpenFOAM model. The coating is assumed to be 12 µm thick (Aslannejad et al., 2017; Aslannejad et al., 2018a). The varying thickness as described in the paper of Aslannejad et al. (2018a) is not taken into account. Information on the geometry and the mesh of all models can be found in Appendix D.1.

2.3.4 Flow parameters and initial conditions

The Van Genuchten - Mualem (Mualem, 1976; Van Genuchten, 1980) model is used as soil hydraulic model. The hydraulic properties of the coating and fibrous layer are based on papers by Aslannejad and Hassanizadeh (2017), Aslannejad et al. (2017), and Aslannejad et al. (2018a). They are listed in table 2.5. The hydraulic properties of both layers are very different; the saturated hydraulic conductivity is 50000 times larger for the fibrous layer and the capillary pressures of the coating layer are about a hundred times larger than the capillary pressures of the fibrous layer.

TABLE 2.5: Hydraulic properties of the coating and fibrous layer

	θ_r [-]	θ_s [-]	α [µm^{-1}]	n [-]	K_s [µm/s]	l [-]
Coating	0	0.34	7.215e-9	4.5	0.001	0.5
Fibers	0	0.5	6.0e-7	2.8	52.90	0.5

The extreme differences in hydraulic properties have a large impact on the numerical model. The pressure distribution is used as initial condition and is assumed

to be at hydrostatic equilibrium from the bottom of the domain. The corresponding water content should be low, since the domain is initially dry. However, the initial pressure distribution inside the domain should be continuous, so the pressure inside the coating and the fibrous layer at the interface should be equal. An initial pressure is used that corresponds to a really low water content in the fibrous layer, while the water content in the coating is already high. The initial pressure at the bottom of this domain is -202000 mm, which corresponds to an initial water content of 8.89e-05 in the fibrous layer and a water content of 0.08 in the coating layer. This means that the water content in the coating is initially already 23.5% of the saturated water content. To solve this issue, there are also two simulations where only the coating is present. In those cases, the hydraulic head is set at -260000 mm at the bottom, which result in an initial water content in the domain of about 0.036.

All sides of the domain are a no-flux boundary, a constant head boundary with h = 0 mm is used at the wetted area of the water droplet. The cumulative flux through the constant head boundary is used to decide when the total droplet volume has infiltrated. At this moment, the simulation is stopped.

2.3.5 Iteration criteria and time settings

To check if the output is correct, HYDRUS reports a water balance error. This error is reported as an absolute and relative value. The absolute error denotes the change in water volume in the domain at a certain timestep compared the previous water volume and the cumulative fluxes at the boundaries. The relative error is the ratio between the absolute error and the maximum of two other quantities. These two quantities are the sum of all fluxes through the boundaries and the sum of the changes in water content in all cells (Šimůnek et al., 2006). The relative water balance error should ideally be below 1%.

To improve the model output, and yield the lowest possible relative water content, the spatial discretization at the paper surface is small, the initial and minimum timestep are low and some iteration criteria are strict. The exact time discretization and iteration criteria are specified in Appendix D.2. Unfortunately, these settings slow down the model significantly, resulting in a runtime that varied between 15 - 100 minutes for one simulation.

3 Results

3.1 OpenFOAM results

In this section, the results of the OpenFOAM model are presented. The output is quantified with the use of the software Paraview (Ayachit, 2015). For all postprocessing steps, the interface between the fluid and air is assumed to be at an α-value (as in eq. 2.4) of 0.5. However, it should be noted that the interface is never perfectly sharp (see figure 3.1), so there are several cells that define the interface and have an α-value between 0 and 1.

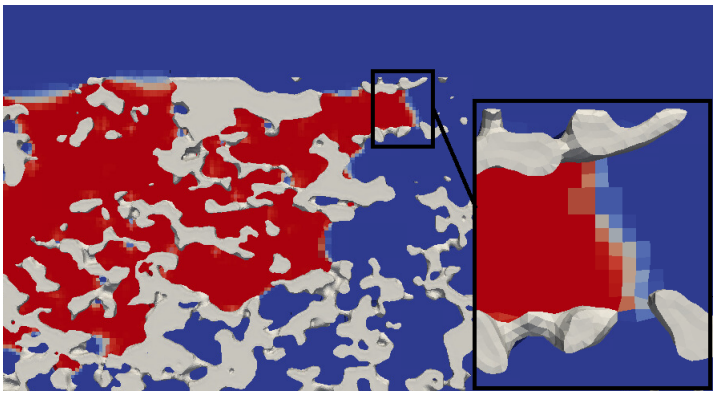

FIGURE 3.1: Side view of final water droplet imprint. A red cell contains an α-value of 1, a blue cell shows $\alpha = 0$. All other shades are an α-value between 0 and 1

An example of droplet infiltration is shown in figure 3.2. For all simulations, the droplet is initially a sphere that is slightly touching the paper surface. Next, it will spread out over the surface, and start to infiltrate the coating. The maximum spread on top of the paper is reached after a few timesteps (middle figures in figure 3.2). Next, the droplet base at the surface shrinks and the simulation continues until the droplet is fully imbibed by the coating.

Since the model output is a 3-dimensional image that also changes over time, keep in mind that all results are a limited representation of the 3-dimensional process. The most useful information with regard to inkjet printing is the final distribution of the water or ink. This includes the distribution inside the coating at the final timestep, but also the data regarding the maximum spreading at the paper surface. The latter is important, as the ink pigments or dye will mainly be deposited here and will make up the final printed image. The movement inside the coating is mainly important to understand the behavior of ink. This information could be used to determine the minimum volume of ink that is necessary to reach an acceptable end result. Lastly, the increase in water content inside the coating will be reported, which will indicate the droplet infiltration rate.

The time scale of total absorption of the droplets varies between 10-100 µs, which is much faster compared to the expected absorption times. In literature, reported absorption times are in the order of milliseconds, although the droplet sizes are slightly larger (Kettle et al., 2010; Tan, 2017). Therefore, it is assumed that the times that are reported by OpenFOAM are incorrect and the duration of all simulations will only be compared to each other.

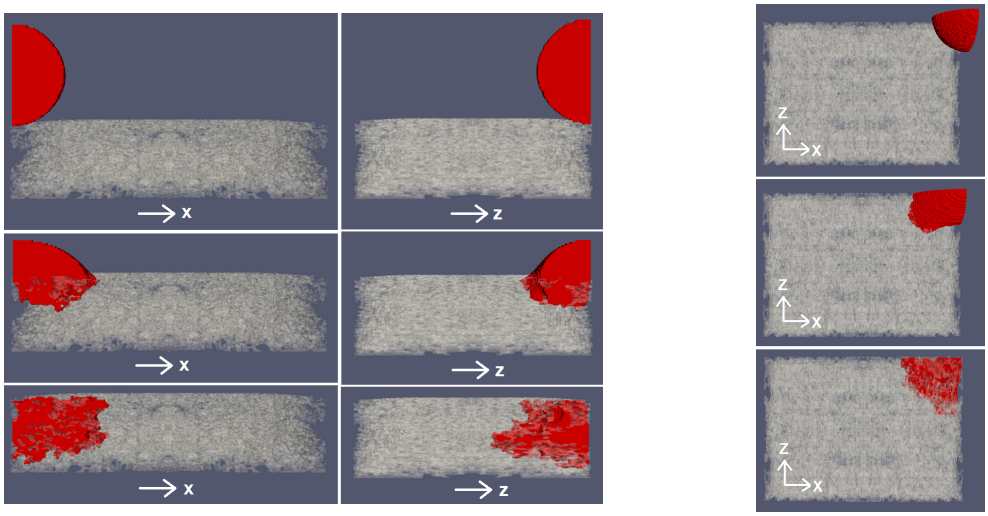

FIGURE 3.2: Infiltration of a water droplet into the paper coating. Top to bottom: initial condition, maximum surface spreading, final imprint. Note that the coating is transparent in the figures.

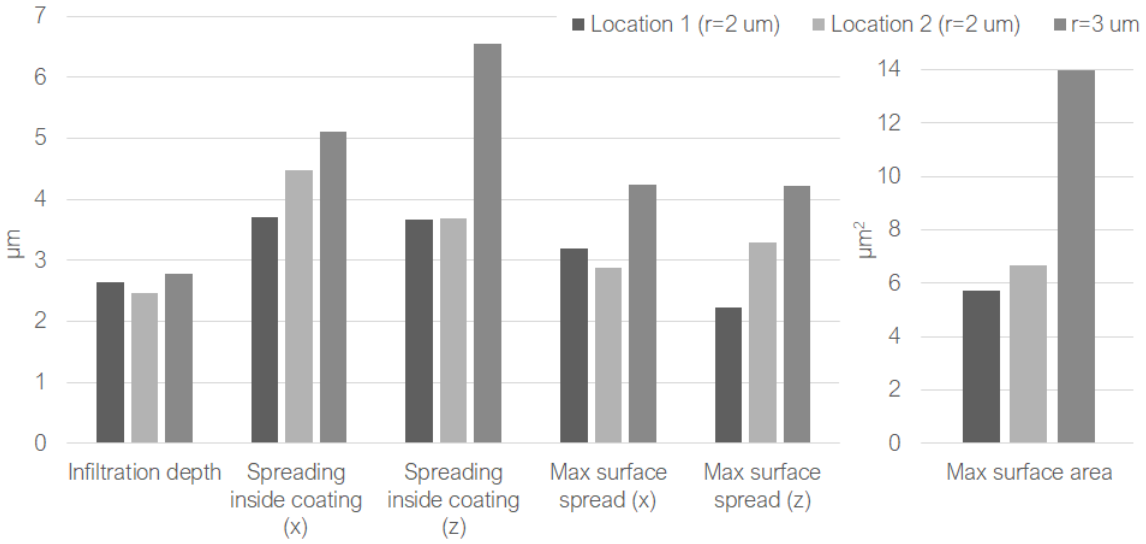

FIGURE 3.3: Results of the model validation. Location 1 is a water droplet of 2 µm at the location of all other simulations. r=3µm is placed at the same location. Location 2 is a water droplet that has infiltrated at another corner.

3.1.1 Model validation

Three cases are considered to validate the model: two cases with a small (r = 2 µm) droplet at different locations and one case with a larger (r = 3 µm) droplet. Figure 3.3 shows the spreading of two equal sized water droplets at different locations. Table 3.1 lists the data of these simulation and the data for the infiltration of a water droplet of 3 µm. This data is also visualized in figure 3.3.

The spreading extent of the two smaller droplets differs for the two locations. Figure 3.3 shows that the maximum spreading both inside the coating as on the surface is different for both locations. The most obvious difference is the maximum surface spreading in Z-direction, with a difference of 1.1 µm.

The difference in volume when regarding the larger droplet is 80 µm^3 (for a full droplet), which means that the larger droplet is 3.5 times larger by volume. The wetted surface area is about 2.5 times larger for the larger droplet, whereas the infiltration depth is similar for both droplets. Especially in the z-direction (both on the surface as inside the coating) the spreading increases with increasing droplet size.

For all three simulations, the fraction of the droplet that has infiltrated the paper coating is plotted in figure 3.5a. Furthermore, the absolute infiltrated volume for the small and large droplet is plotted over time in 3.5b.

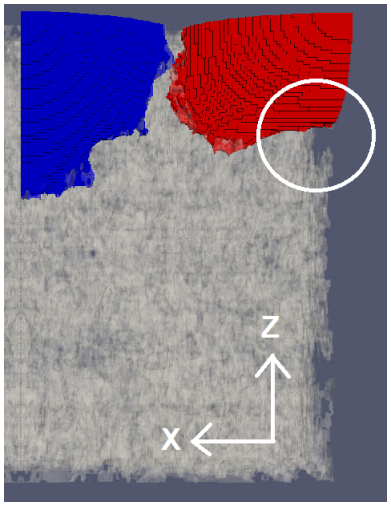

FIGURE 3.4: Comparison of the maximum spreading on the coating surface at two locations. Red: location 1 (the location of all other simulations). Blue: location 2. The coating is transparent. White circle: large pore that inhibits flow.

TABLE 3.1: Infiltration and spreading of all validation simulations. The first three columns denote the final lengths in three directions inside the coating layers. The second three columns show the maximum spreading at the surface. The last column shows at what time the maximum surface spreading occurs. Location 1 (r=2 µm) the position of all other simulations. The large droplet (r=3 µm) is also placed at location 1.

	Inside coating			**On surface of coating**			
	Infiltration depths (µm)	**x** (µm)	**z** (µm)	**Max area** (µm^2)	**x** (µm)	**z** (µm)	**Time** (µs)
Location 1 (r=2 µm)	2.64143	3.71606	3.6732	5.72567	3.19949	2.2233	2.5
Location 2 (r=2 µm)	2.45546	4.47891	3.69062	6.6611	2.87856	3.3015	2.5
Radius = 3 µm	2.77575	5.11078	6.54922	13.99	4.23821	4.22987	5

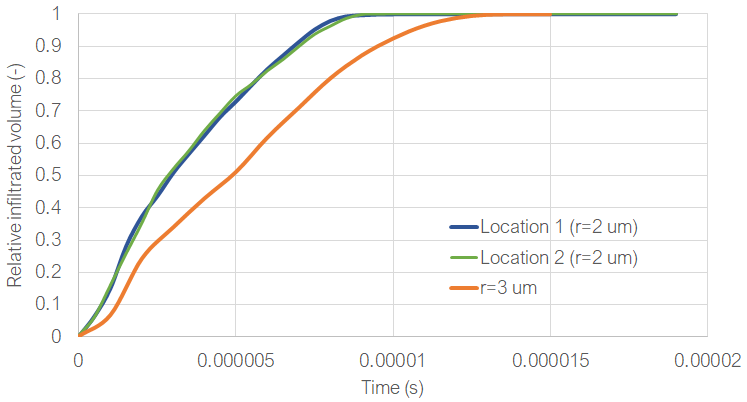

(A) Relative infiltrated volume of all validation simulations. The y-axis shows the fraction of the droplet that is inside the coating layer.

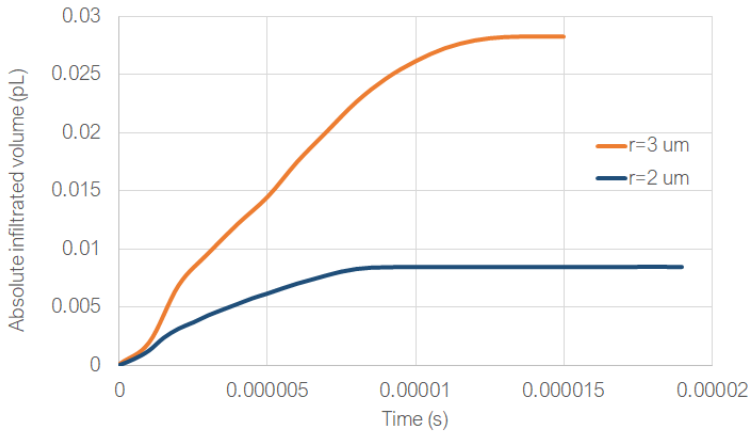

(B) Absolute infiltrated volume of a droplet of radius 2 and 3 µm.

FIGURE 3.5: Infiltration over time for the model validation simulations.

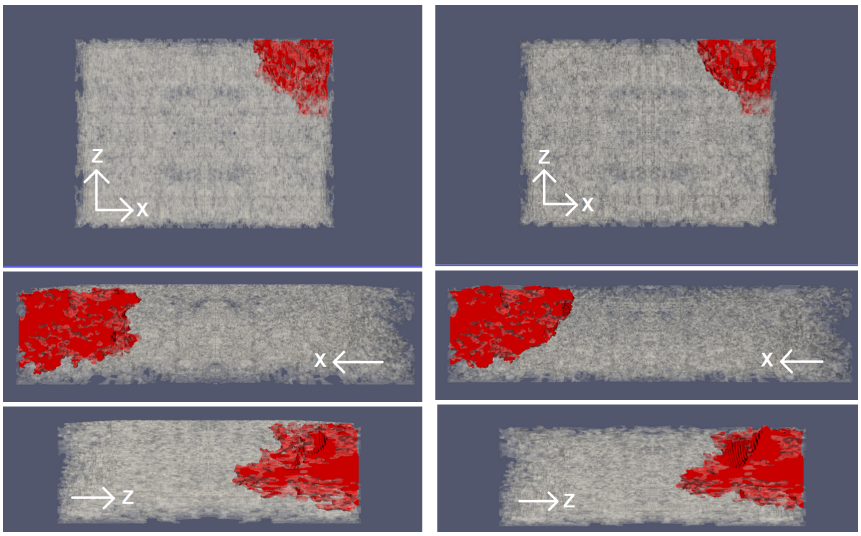

FIGURE 3.6: Comparison of the final imprint of a water (left) and ink (right) droplet. The coating layer is transparent.

3.1.2 Parameter study

This section shows the results of the parameter study. Table 3.2 contains the general results of every simulation. The first three columns show the infiltration depth, this data is derived at the final timestep of the simulation. The last four columns present the lateral spreading on top of the surface. As shown in figure 3.2, the maximum spreading at the surface is reached during the first few timesteps, after which the droplet base at the surface starts to shrink again. The values in the last columns of table 3.2 are derived when the maximum wetted surface area was reached. The corresponding time is shown in the last column

When regarding the results of all OpenFOAM simulations, it becomes obvious that a change in fluid properties will have little effect on the final imprint of a droplet. Moreover, whether an ink-like droplet or a water droplet is placed on a paper coating, will have hardly any effect on the surface area and infiltration depth. An exception to this is a changing contact angle; these simulations show a distinct difference in surface area and infiltration depth.

Although the maximum imprint measured in three directions is almost equal for every simulation, the imprints may still be slightly different. To illustrate, the final imprint of a water and an ink-like droplet is shown in figure 3.6. According to table 3.2, the final imprint in x-direction is almost the same, while in figure 3.6, the shape in the x-direction is different for both simulations.

TABLE 3.2: All data regarding infiltration and spreading. The first three columns denote the final lengths in three directions inside the coating layers. The second three columns show the maximum spreading at the surface. The last column shows at what time the maximum surface spreading occurs.

	Inside coating			**On surface of coating**			
	Infiltration depths (µm)	**x** (µm)	**z** (µm)	**Max area** (µm^2)	**x** (µm)	**z** (µm)	**Time** (µs)
Ink-like liquid	2.51967	3.71766	3.657	5.72642	3.19949	2.19878	13
Water	2.64143	3.71606	3.6732	5.72567	3.19949	2.2233	2.5
Intermediate density (30% glycerol)	2.51421	3.71606	3.6732	5.70267	3.19949	2.19878	3.5
High density (60% glycerol)	2.64143	3.71606	3.6713	5.72151	3.19949	2.19878	4
Intermediate viscosity (30% glycerol)	2.51967	3.71606	3.58042	5.72532	3.19949	2.19878	8.5
High viscosity (60% glycerol)	2.74098	3.71606	3.6732	5.72617	3.19949	2.19878	41
Low surface tension	2.51967	3.71606	3.6732	5.72992	3.19949	2.19878	5
Contact angle: 1°	2.925	4.04139	4.00256	6.19848	3.24714	2.2233	2
Contact angle: 90°	0.328607	2.1714	1.77553	2.88851	2.16754	1.77561	3.5
Impact velocity	2.64143	3.71606	3.6713	5.75772	3.19949	2.22696	2

Figure 3.7 shows the total water content inside the coating over time for every simulation. The value on the y axis shows fraction of the whole pore space volume that contains water. With the use of this graph, the infiltration rates for every simulation can be compared. The droplet with a 90° contact angle did not fully infiltrate, which is why the water content remained at 0.003. Note that the total volume of the droplet is about 10% of the pore space volume, so the droplet is fully infiltrated when the water content is 0.1. A more detailed look on the plots can be found in appendix E, where the graph is split for the separate fluid properties. The term 'water content' will be used as a general expression for the fluid fraction in the simulations. The plot of water content of the high viscosity simulation is cut off, as the duration of its infiltration was much longer compared to the other runs. The full graph of the water content of the high viscosity run is shown in figure E.3.

The differences in water content are much more distinct compared to the differences in imprint. Compared to the infiltration of a water droplet, most simulations will have a slower infiltration: only an impact velocity and a 1° contact angle will result in a higher infiltration rate. An increase in fluid density will have a relatively small impact on the infiltration rate, whereas an increase in viscosity will slow down the infiltration extensively. Also, decreasing the surface tension by approximately a factor two results in a slower infiltration.

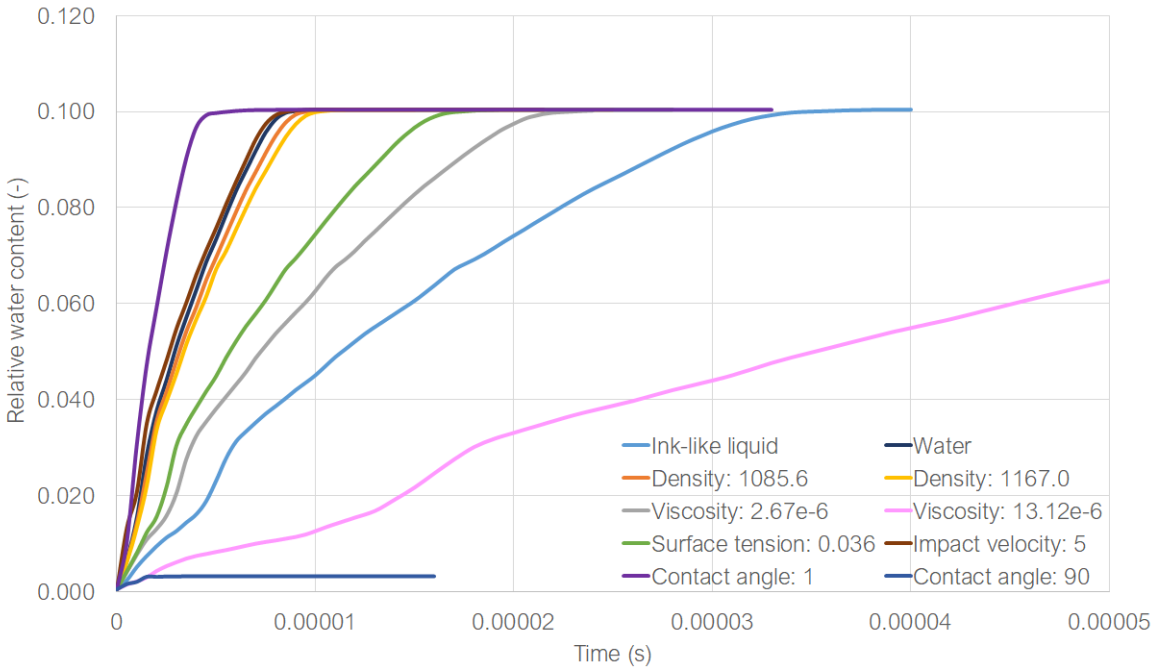

FIGURE 3.7: Water content inside the coating layer for all simulations of the parameter study. Note that the graph of high viscosity is cut off to be able to distinguish the differences at lower times.

In the next sections, the infiltration depth and wetted surface area is plotted over time for all simulations of the parameter study. The plot of wetted surface area is the area of the droplet base on the paper surface. The droplet eventually fully infiltrates the paper coating, so the droplet at the surface will become depleted. Hence, the surface area for all simulations will eventually decrease. For most simulations, eventually the same infiltration rate and spreading area will be reached, which is described in table 3.2. However, the plots in the next sections clearly indicate that the time until maximum spreading and depth is varying when fluid properties are changed.

Contact angle and surface tension

Changing the contact angle will influence the maximum infiltration depth and maximum spreading rate. A droplet with a contact angle of 90° only infiltrates and spreads slightly until it reaches a steady state and does not move anymore. A droplet with contact angle 1° spreads almost as fast as a droplet of 45°, but it reaches a higher maximum area. The infiltration of a 1° contact angle into the coating is faster and the maximum infiltration depth is higher compared to a 45° droplet.

The low surface tension droplet has half the surface tension but the same contact angle as a pure water droplet. The maximum wetted area for this droplet is equal to that of a water droplet, the maximum infiltration depth is slightly lower compared to water. The duration of spreading and infiltration is much higher compared to water.

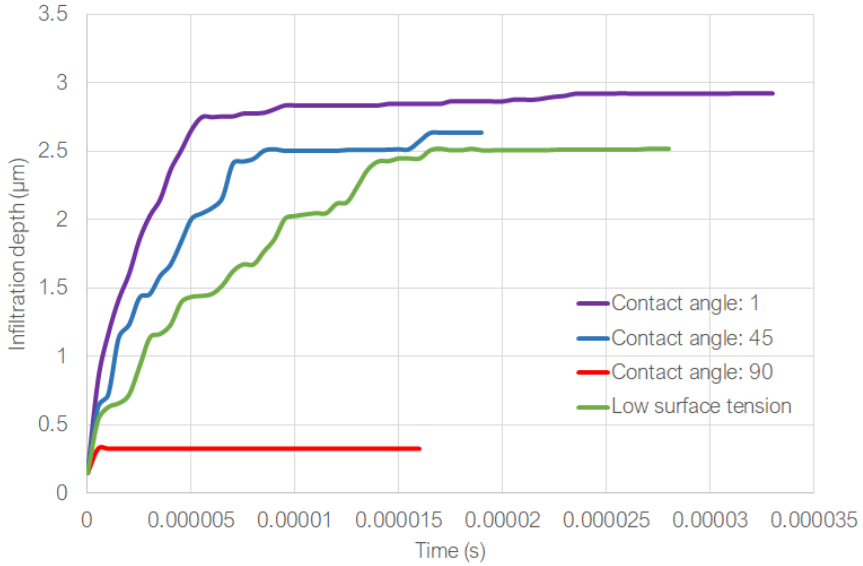

(A) Maximum infiltration depth

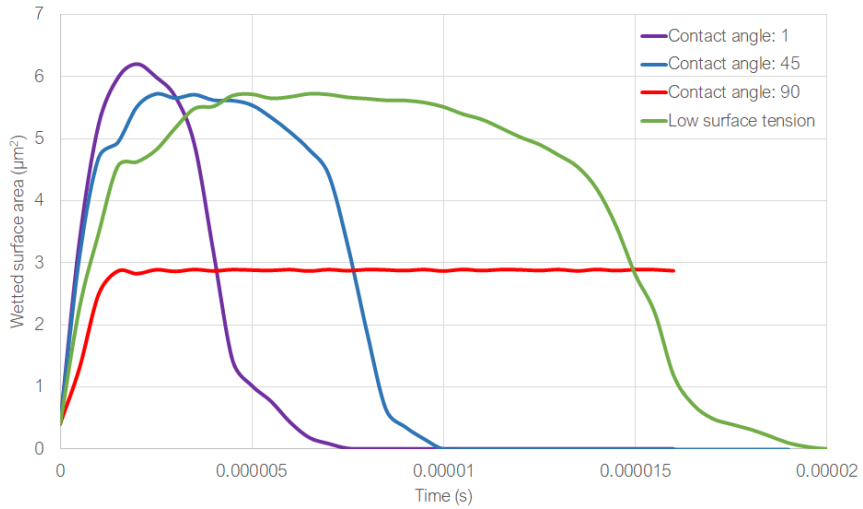

(B) Surface area

FIGURE 3.8: Infiltration and spreading over time for droplets with a different contact angle or surface tension. The plot of a 45° contact angle shows the infiltration of a pure water droplet (σ = 0.072 kg/s^2). The low surface tension droplet has a contact angle of 45° and σ = 0.03571 kg/s^2.

Viscosity

An increase in viscosity has a big impact on the spreading and infiltration of a droplet. The maximum contact area on the paper surface of the three droplets is the same; the infiltration depth for a high viscous droplet is slightly higher. The speed of the processes decreases significantly for an increasing viscosity.

The surface area plot of the intermediate viscosity simulation shows that the final surface area is above 0, so the simulation was stopped before the droplet was fully infiltrated.

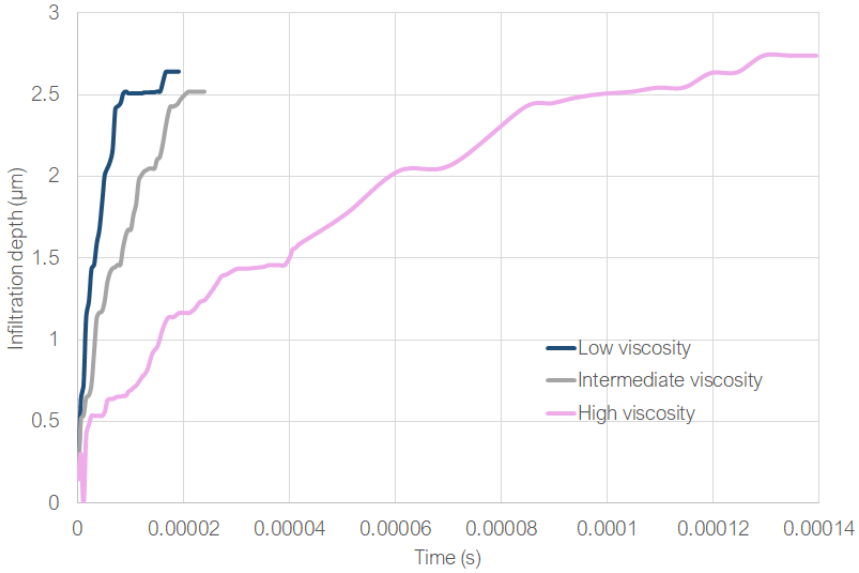

(A) Maximum infiltration depth

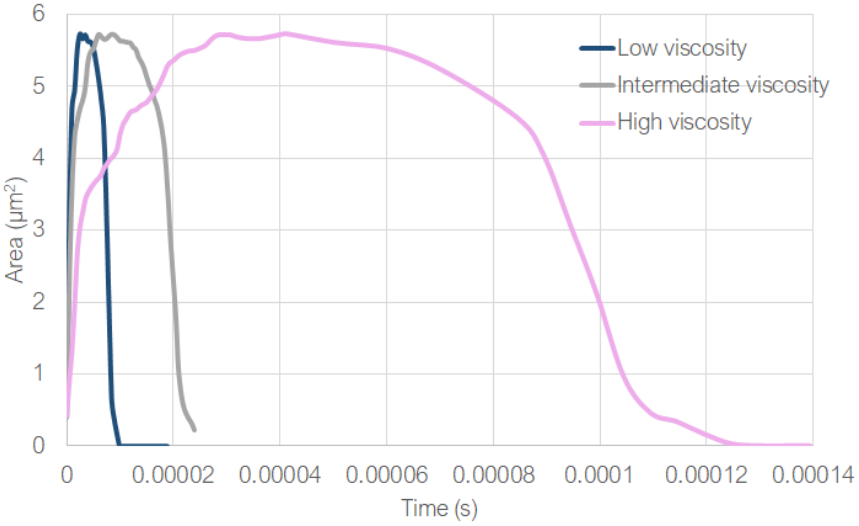

(B) Surface area

FIGURE 3.9: Infiltration and spreading over time for a changing viscosity: low viscosity = 1e-6 m^2/s, intermediate viscosity = 2.6739e-6 m^2/s, high viscosity = 13.117e-6 m^2/s, The low viscosity plot shows the infiltration of a pure water droplet.

Density

Changing the density has a small impact on the final infiltration depth, wetted surface area and the rate at which these processes occur. The graphs in figure 3.10a are very similar, but the total increase in water content inside the coating is increasing a little more slowly when the density increases (as seen in figure 3.7 or E.4).

The initial spreading of the three simulations are almost equal, but the decrease in wetted surface area is occurring more slowly with increasing density. The low and high density droplets eventually reach the same infiltration depth, but the simulation of the low density simulation was already terminated before the last increase might have occurred.

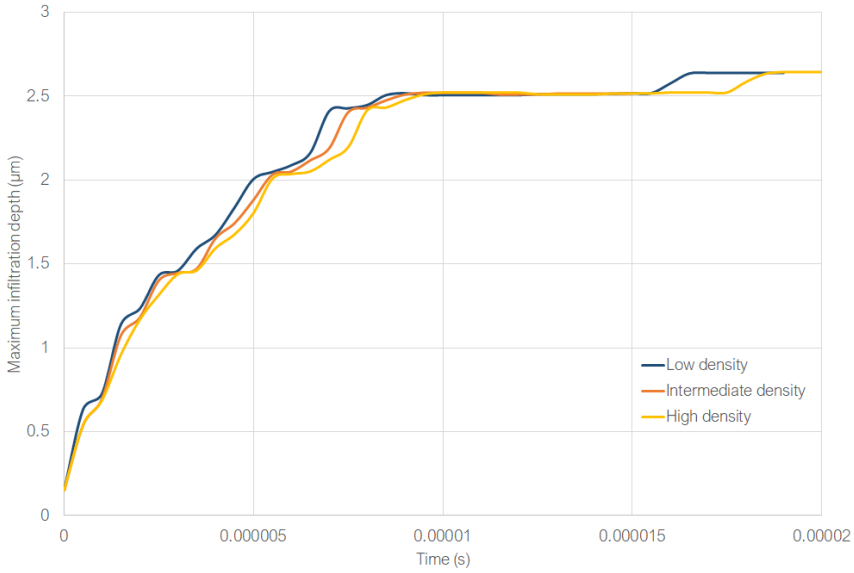

(A) Maximum infiltration depth

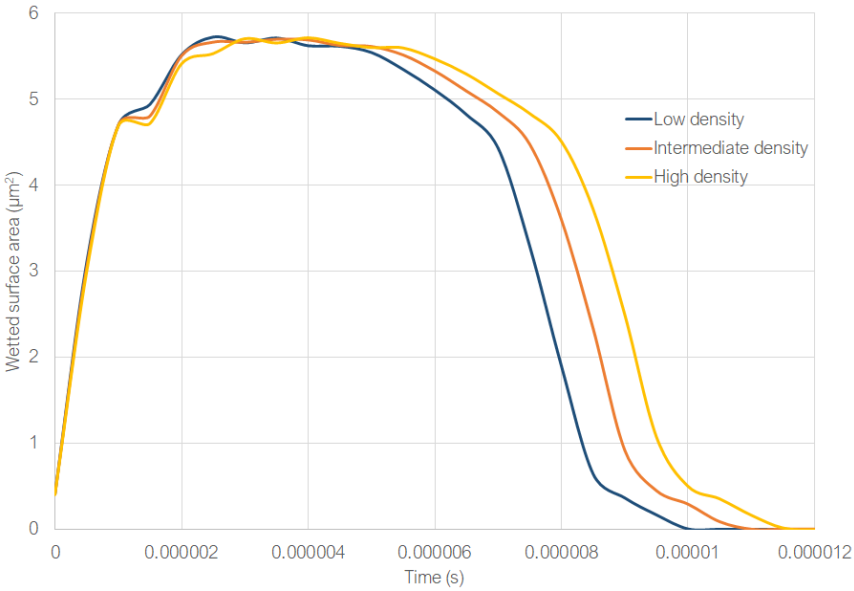

(B) Surface area

FIGURE 3.10: Infiltration and spreading over time for a changing density: low density = 1000 kg/m^3, intermediate density = 1085.6 kg/m^3, high density = 1167 kg/m^3. The low density plot shows the infiltration of a pure water droplet.

Impact velocity

The plots of infiltration depth over time for a sessile ($v = 0$ m/s) droplet or a droplet that has an initial velocity of 5 m/s are almost the same. The increase in water content inside the coating is slightly faster for a droplet with an impact velocity (see figure 3.7 or E.2), so the infiltration rate is higher for higher impact velocities.

The maximum wetted surface area is a little higher for the droplet with a velocity of 5 m/s. This maximum area is also reached earlier, so the spreading rate also increases for an increase in impact velocity.

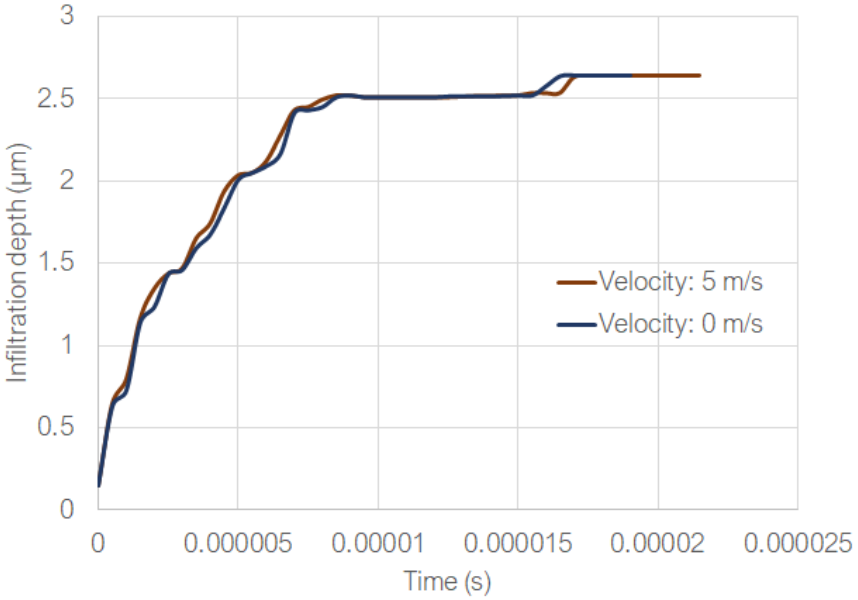

(A) Maximum infiltration depth

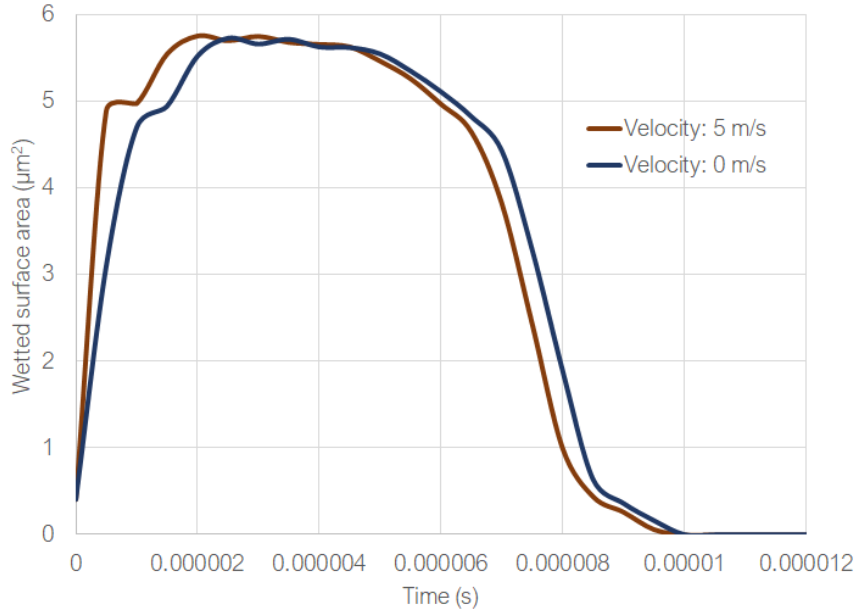

(B) Surface area

FIGURE 3.11: Infiltration and spreading over time for droplets with and without an impact velocity

Water and ink-like fluid

In this study, an ink-like fluid is simulated by changing the density, viscosity and surface tension compared to pure water (see also table 2.4). The contact angle of both liquids is kept the same. The imprint for a water and ink-like droplet are very similar; they have practically the same maximum wetted area and the water droplet has infiltrated only 0.1 µm deeper. However, the spreading and infiltration of an ink-like droplet takes place significantly slower compared to the infiltration of a water droplet. As shown in figure 3.7, the simulation of an ink-like liquid even shows the slowest infiltration, except for a droplet with a very high viscosity (13.117e-6 m^2/s).

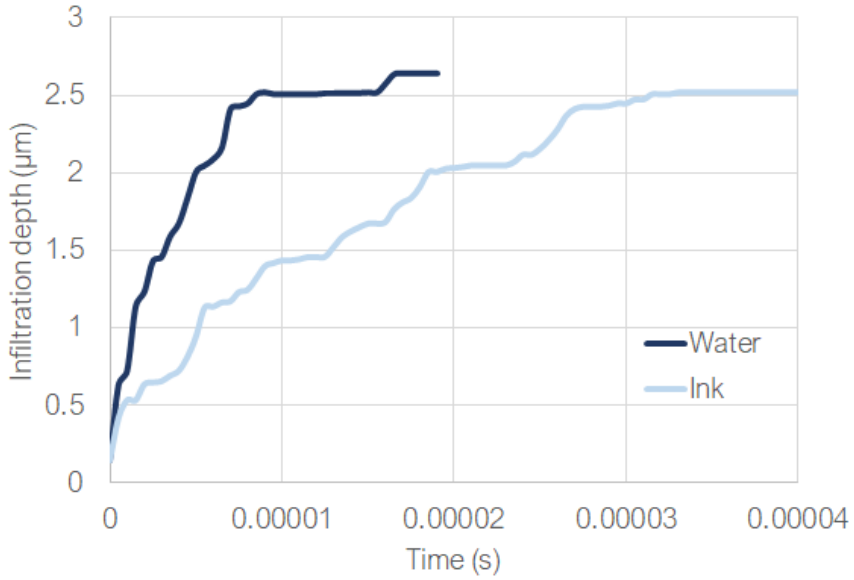

(A) Maximum infiltration depth

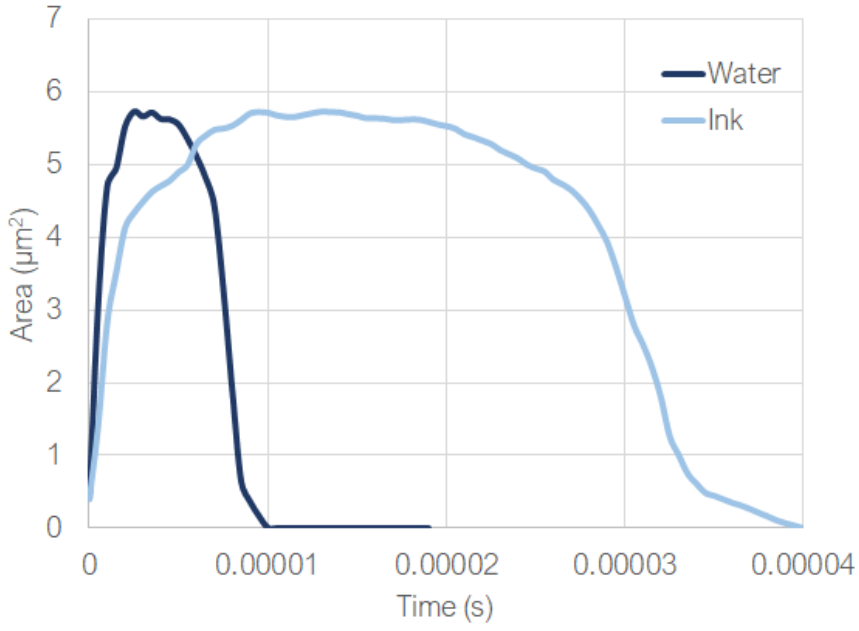

(B) Surface area

FIGURE 3.12: Infiltration and spreading over time of a water and ink-like droplet

3.2 HYDRUS results

In this section, the results of the three cases of the HYDRUS model are shown. The general data is listed in table 3.3. This table also contains the relative water balance error, which was explained in section 2.3.2. The relative water balance error should be below 1%. However, the water content in this model is initially really low and the boundary fluxes are really small, hence the relative error is often slightly higher than 1%, especially at the beginning. The maximum error is occurring during the first timestep for the small droplet simulation and coating+fibers simulation. This is reasonable, because the domain is initially very dry and the pressure difference between the boundary and the domain is large. However, the maximum watBalR of the 20 µm droplet into the coating reaches its maximum error after 0.0014 seconds.

The infiltration flux for the three cases is shown in figure 3.13. The infiltration at the constant head boundary is constant at every node, so the total flux is higher for a contact radius of 20 µm. The irregular pattern shown in the plots of the large droplet infiltration (fig. 3.13a) is caused by a saving error of HYDRUS and has nothing to do with the results itself. Furthermore, there is an error in the initial flux for the small droplet case, as can be seen on the left edge in figure 3.13b: the flux starts negative and then becomes really high before it follows a normal curve. This is also reflected in the high water balance error at the beginning of infiltration of the small droplet (see table 3.3).

The increase in infiltration flux for the large droplet into the coating only also corresponds to an increase in water balance error, that is highest at t = 0.0014 seconds.

TABLE 3.3: Results of the three HYDRUS simulations and the maximum and minimum relative error.

	Time until infiltration (s)	**Maximum infiltration depth** (µm)	**Maximum lateral spread** (µm)	**Maximum watBalR** (%)	**Minimum WatBalR** (%)
Coating					
3 µm droplet	3.77E-05	5.528	8.148	31.42	0.133
20 µm droplet	0.00358	12	60.8	5.798	0.355
Coating + fibers					
20 µm droplet	0.00375	12	75.95	6.266	3.552

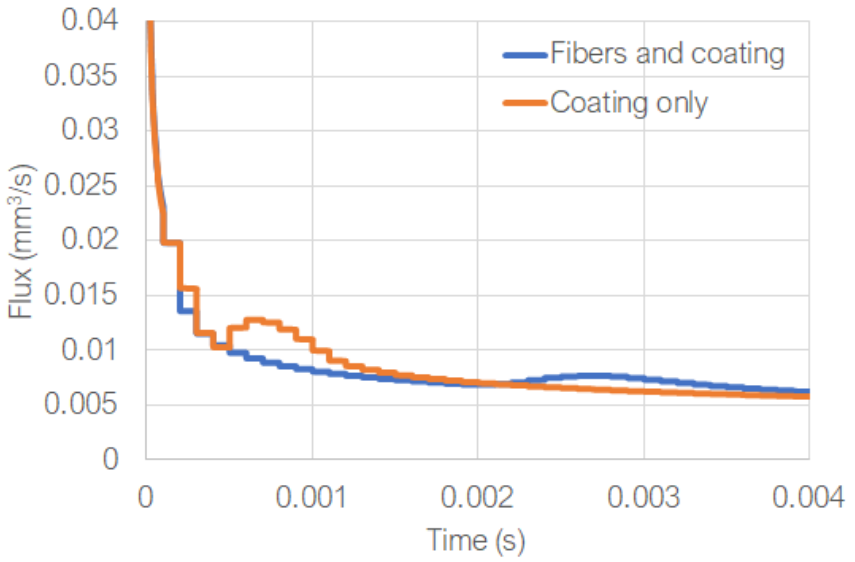

(A)

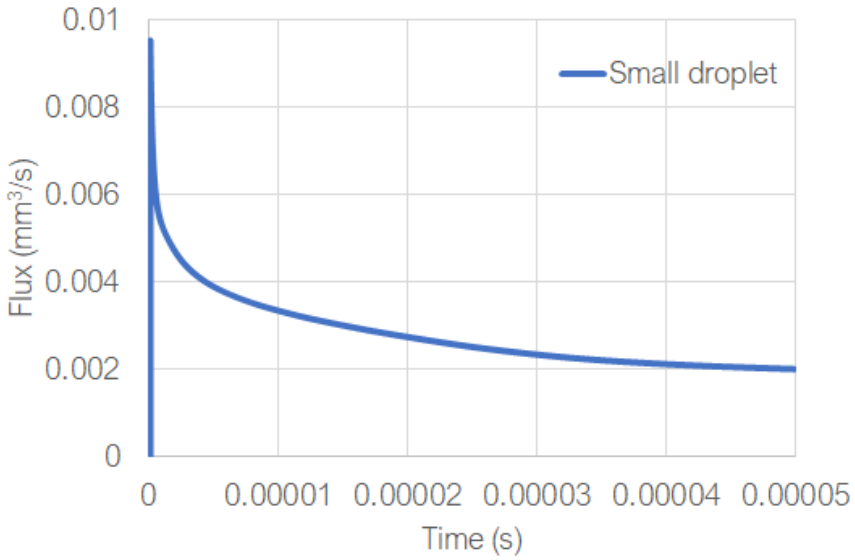

(B)

FIGURE 3.13: Flux through the constant head boundary, at the location of the droplet on the paper surface. A) Infiltration of a large droplet ($r = 20$ µm) into a coating layer and a coating layer on a fibrous layer. B) Infiltration of a small droplet ($r = 3$ µm) into the coating.

3.2.1 Large droplet

The behaviour of the large droplet that is infiltrating the coating is shown graphically in figure 3.14 and plotted in figure 3.15. The plot of the water content in horizontal direction is measured just below the paper surface, for the vertical direction it is measured at the left boundary of the domain.

The water reaches the bottom of the coating after 0.00024 s. After 0.00088 s (not shown in the figures), the saturation front is vertical. According to figure 3.15a, the final saturated imprint is at 30 µm, so it only extends 10 µm beyond the original wetted radius. However, the region between 30 and 59 µm is unsaturated. Comparing the first and last plot in figure 3.15a, it becomes clear that the unsaturated part increases over time, while the saturated part only slightly extends beyond the original droplet radius.

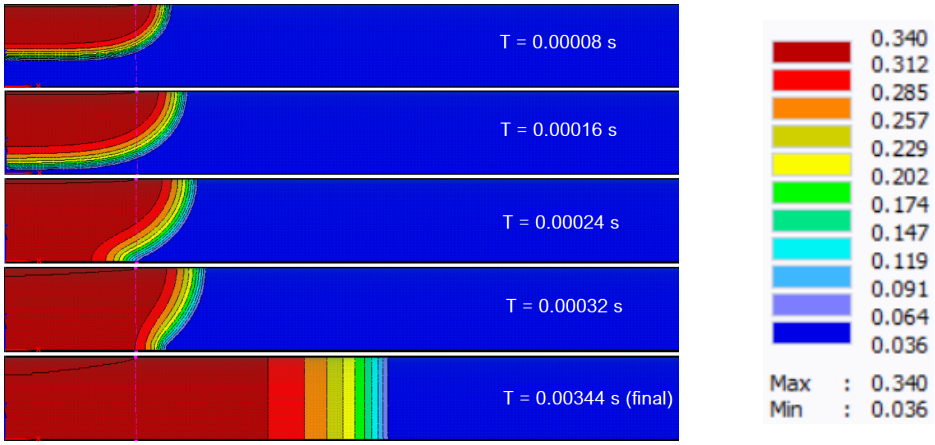

FIGURE 3.14: Water content over time during infiltration of a large droplet (r = 20 µm) into the paper coating. The pink dotted line shows the droplet radius at the top boundary. The bottom image shows the final distribution of water. The dimensions are 100 µm in x-direction and 12 µm in z-direction.

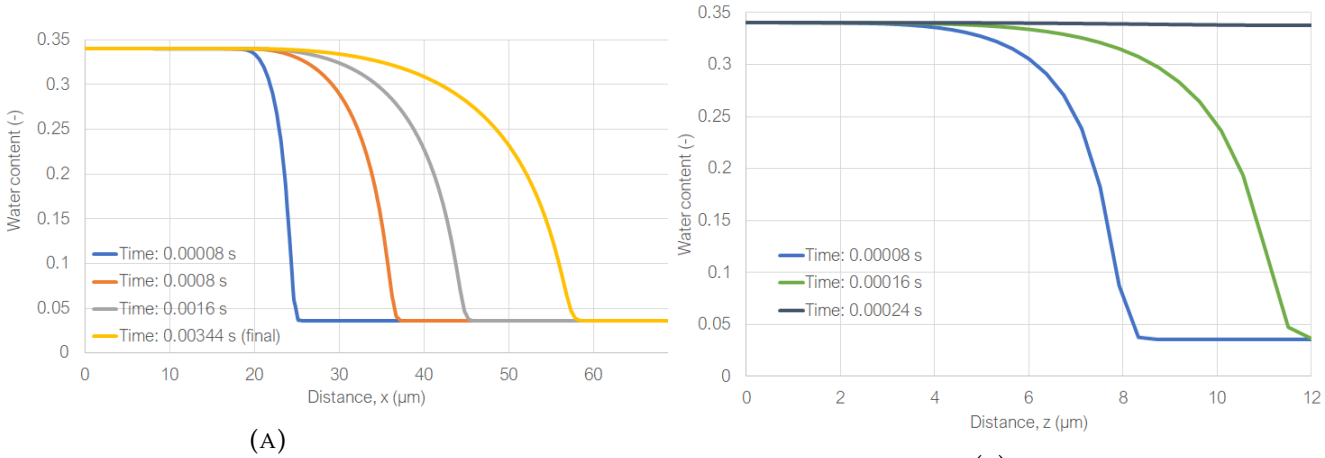

(A) (B)

FIGURE 3.15: Water content in horizontal and vertical direction inside the coating during infiltration of a large droplet (r = 20 µm) at different timesteps. The values on the x-axes denote the distances from the left boundary (A) and the paper surface (B). The yellow curve (A) is the imprint after droplet infiltration, the vertical distribution remains constant after T = 0.00024 s.

3.2.2 Small droplet

The behaviour of the small droplet that is infiltrating the coating is shown in figure 3.16 and plotted in figure 3.17. The plots are measured at the same locations as the large droplet case. Note that the coating thickness is equal to the thickness of the domain of the large droplet infiltration (12 µm).

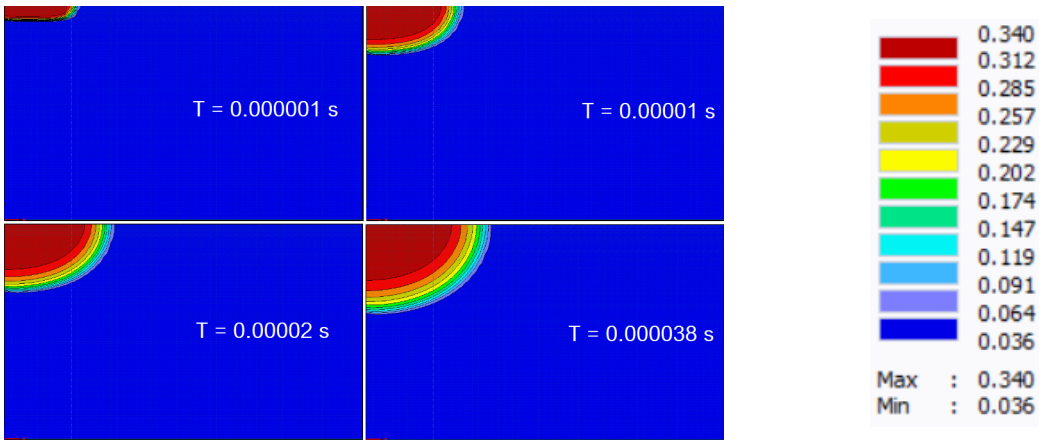

FIGURE 3.16: Water content over time during infiltration of a small droplet (r = 3 µm). The pink dotted line shows the droplet radius at the top boundary. T = 0.000038 s corresponds to the final imprint after the full droplet has infiltrated. The dimensions are 20 µm in x-direction and 12 µm in z-direction.

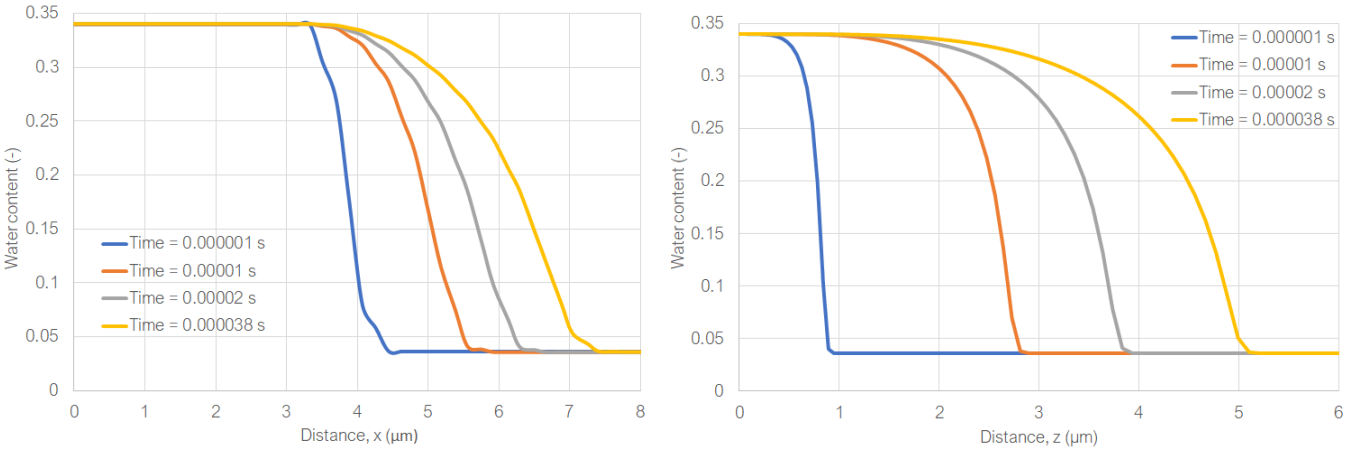

(A) (B)

FIGURE 3.17: Water content in horizontal and vertical direction inside the coating during infiltration of a small droplet (r = 3 µm) at different timesteps. The values on the x-axes denote the distances from the left boundary (A) and the paper surface (B). The yellow curve is the imprint after droplet infiltration.

3.2.3 Coating and fibers

The final infiltration into the coating layer on top of the fibrous layer is shown graphically in figure 3.18. The left part shows the imprint in the whole domain, although the right side is cut off. The right image shows that the water content inside the fibrous layer is slightly increased at the end of the droplet infiltration, although the water content is still very low. The results are also plotted in 3.19. The right plot shows that the coating layer is saturated after 0.00024 seconds, but that the water content inside the fibrous layer only starts to increase after 0.0012 seconds.

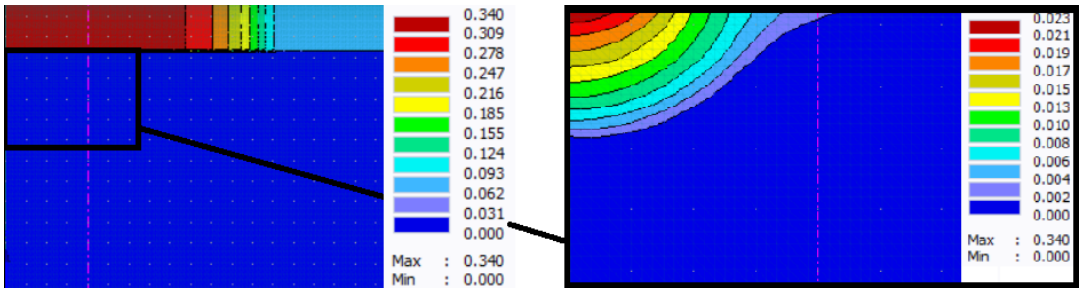

FIGURE 3.18: Final imprint inside the coating and fibers. The pink dotted line shows the droplet radius at the top boundary. Note that the scales of both figures is different.

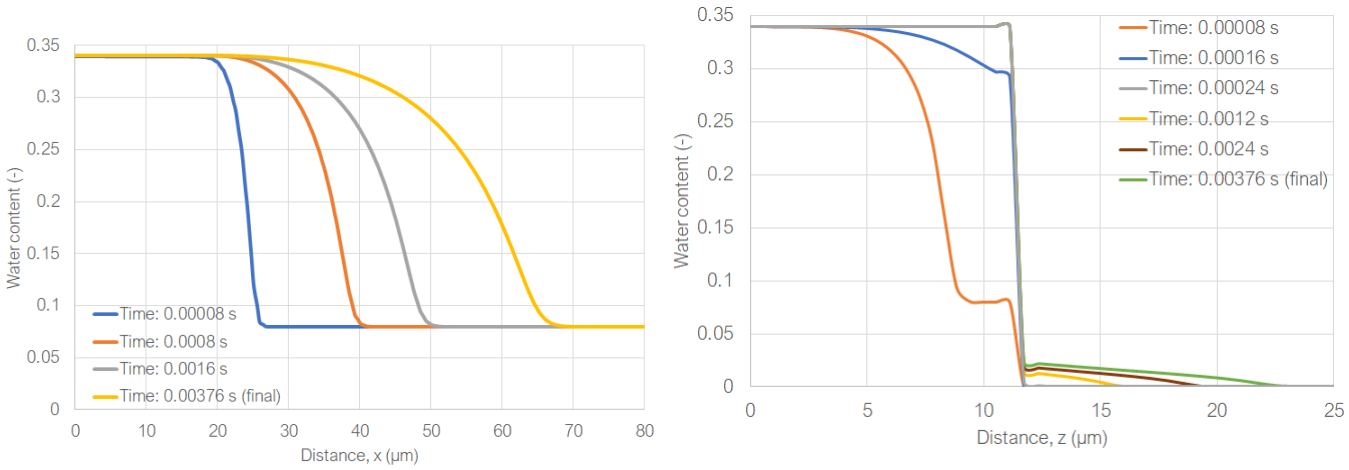

(A) (B)

FIGURE 3.19: Water content in horizontal and vertical direction inside the paper during infiltration of a large droplet (r = 20 µm) at different timesteps. The values on the x-axes denote the distances from the left boundary (A) and the paper surface (B). The yellow curve (A) and green curve (B) is the imprint after droplet infiltration. The top of the fibrous layer is situated at 12 µm.

4 Discussion

In this chapter, the results of the pore-scale model and the continuum-scale model will be discussed. A technical discussion of the OpenFOAM model contains an overview of simplifications and possible improvements of the pore-scale model. After discussing the results of both models separately, the models will be compared to each other to decide which model is better in describing the infiltration of small droplets into the coating layer of paper. The last section lists some possibilities for future research.

4.1 OpenFOAM

4.1.1 Droplet position

The spreading and infiltration of two equal sized droplets is different when the droplet is placed at another location, as shown in figures 3.3 and 3.4. This means that, at least for a 2 µm radius droplet, the behaviour inside and on top of the paper coating is influenced by local pore structure. This effect can be seen in figure 3.4, a large pore is inhibiting the droplet at location 1 (red) to spread further over the coating. As already was noted in the theoretical background (section 1.2.2), this behaviour was also observed in other studies (Schoelkopf et al., 2000; Ridgway et al., 2002). These studies argued that the inertia of the fluid inhibits the infiltration in the largest pores.

Furthermore, figures 3.2 and 3.3 illustrate that a droplet on and inside the coating does not spread perfectly radial. The maximum distances in x- and z-direction are not equal: compare for example the final spread in x- and z-direction for the droplet at location 2. This also illustrates the effect that the local pore structure can have on the distribution of water.

The plots of relative infiltrated volume (see figure 3.5a) show that the infiltration rate is equal for both locations. Moreover, according to table 3.1, the maximum surface area is reached at the same time for both locations. Therefore, it can be concluded that the rate at which the processes occur, is not influenced by the position of the droplet and the pore structure at that location.

4.1.2 Droplet size

The infiltration of the larger droplet (r = 3 µm) can be roughly compared with the satellite stains that were created during the experiments. The diameters of satellite stains were 6 µm and 10 µm and the infiltration depths were 2 µm and 3 µm respectively (see table 2.2). The exact volume of the satellite droplets cannot be determined. The infiltration depth in OpenFOAM is 2.77 µm and the spread in two directions on top of the coating is about 4.2 µm (see table 3.1). These results are similar to the measured extents, so it can be concluded that the results are valid.

Especially in the z-direction (both on the surface as inside the coating) the spreading increases with increasing droplet size. This means that the water also spreads

over and into the large pore that remained unfilled during infiltration of the small droplet (indicated with a circle in figure 3.4). As a result, the spreading of the 3 µm droplet is much more radial compared to that of the 2 µm droplet.

The infiltration depth is almost equal for both droplet sizes. The values for lateral spreading inside the coating layer clearly show that the fluid movement took place more laterally instead of vertically inside the coating. This can be explained by the large increase in surface area, which means that there is a larger area over which infiltration can occur, which means that the fluid inside the coating layer will also spread out more evenly. This means that an increase in droplet volume will have a much larger effect on the spreading compared to the infiltration. This behaviour is comparable with the results of Fu et al. (2019). Their modelling showed that larger droplets will spread more, while the size increase hinders the infiltration. However, according to their research, the infiltration depth decreased significantly, whereas the depth in this study remained the same.

The infiltration rates can be compared with figures 3.5a and 3.5b. The first figure shows the fraction of the total droplet volume that is inside the coating layer. It will take longer before the larger droplet is fully imbibed by the coating layer, because the volume is larger. The second figure shows the absolute volume inside the coating layer over time, which indicates that the infiltration rate is higher for the large droplet. Due to the larger wetted surface area, infiltration of the larger droplet can also occur over a wider area. For a smaller droplet, this area is smaller and the infiltration will slow down due to the friction of the fluid inside the porous structure. Tan (2017) also observed this increase in infiltration rate in their experiments with droplets of 10 - 220 pL.

4.1.3 Contact angle

According to table 3.2, the simulations with different contact angles are the only runs that show a significant difference in infiltration depth and maximum surface area compared to the other simulations. The evolution of infiltration depth and surface area over time for these simulations is shown in figure 3.8. It is important to note that the surface tension between the liquid and air was kept at the same value for these three simulations. Looking at the Young-Dupré equation (see equation 1.2), this means that a change in contact angle reflects a change in surface tension at the solid-gas and solid-liquid interfaces. In this case, a change in contact angle therefore reflects a change in hydrophilicity of the paper coating. In that sense, the changing contact angle does not describe a change in fluid properties, but a change in properties of the porous medium.

A fluid with a high contact angle (90°) will not be imbibed by the coating, although it slightly infiltrates the pores at the coating surface. Furthermore, it spreads out slightly over the surface, but becomes immobile soon after.

A fluid with a low contact angle (1°), will result in an increase in maximum surface area and infiltration depth. The infiltration rate also increases, but the rate of spreading is not influenced by a decreasing contact angle. The latter is shown in figure 3.8b, where the plots of contact angles 1° and 45° are initially equal. Due to the increased infiltration rate the fluid with 1° will move very fast into the paper coating, and the surface area decreases much faster compared to the infiltration of water (contact angle 45°).

The increase in infiltration rate is expected, see for example the Laplace capillary pressure equation (eq. 1.1). A decrease in contact angle will result in a higher capillary pressure, which consequently causes the fluid to flow easier into the coating.

This also explains the wide distribution of fluid inside the coating: the width of the imprint inside the coating in x- and z-direction is also higher for a contact angle of 1° compared to a water droplet. The capillary pressure caused the fluid to spread further in all directions.

4.1.4 Surface tension

Closely related to the contact angle is the surface tension of the liquid-air interface. For the simulation where the surface tension (between the fluid and gas phase) is decreased, the contact angle is kept at the same value. However, this means that the surface tension at the solid-gas and solid-liquid interface also have to change (see Young-Dupré equation, eq. 1.2).

In contrast to changing the contact angle, where the change mostly reflects a change in properties of the solid, the change in surface tension (while keeping contact angle constant) shows the combined change in properties in the solid and liquid. It should be noted that it is unlikely that a liquid with a different surface tension will result in the same contact angle when the same coating is used. Nevertheless, this simulation will provide extra information on the results of the ink-like liquid compared to the infiltration of water.

Decreasing the surface tension will cause infiltration and spreading to slow down significantly. This is expected behaviour, since a lower surface tension results in a lower capillary pressure according to the Young-Laplace equation (eq. 1.1),. This means that the wetting force is decreased, while the drag force (equation 1.3) is still the same.

Koivula et al. (2012) reported the effect of the spreading of water and oil droplets over calcium carbonate tablets with different size distributions. They noticed that especially water droplets spread very different over the different tablets. They attributed this effect to the especially high surface tension of water. This means that a slight change in surface structure can strongly influence the spreading behaviour of a droplet with a high surface tension. It would therefore be interesting to see whether changing the surface tension has the same effect when the droplets are infiltrating at another location on the coating layer.

4.1.5 Viscosity

The full plots of the water content inside the coating for droplets with an increasing viscosity are shown in figureE.3 This graph illustrates that the viscosity of a fluid has a large impact on the rate of spreading and infiltration; figure E.3 and 3.9a clearly indicate that a more viscous fluid will infiltrate more slowly. The medium viscous and high viscous fluid will take respectively 2 and 12 times longer to infiltrate compared to water and 3 and 16 times longer to spread. This decrease in flow rate is very predictable, as a higher viscosity will increase the viscous drag at the pore sides.

The infiltration depth is lowest for the intermediate viscosity fluid. However, as already was discussed in the results section, the simulation of an intermediate viscosity is terminated to early. This droplet might have infiltrated further if the simulation had run for a longer time.

The high viscous fluid reaches a relatively high infiltration depth that is 0.1 µm deeper than the infiltration of water. This is striking, as you would expect a low infiltration depth for a high viscosity, because of the presence of high viscous forces that counteract the capillary action.

4.1.6 Density

An increase in density will result in a slightly slower infiltration (see figure E.4 and 3.10a). Eventually, the low and high density droplets reach the same infiltration depth, but the simulation of the intermediate density droplet was already terminated before this point. The infiltration depth of the intermediate density might have eventually reached the same point, if the simulation had run for a longer time.

According to table 3.2, droplet with an intermediate density has a maximum wetted surface area that is 0.02 μm^2 lower than water (with a low density). However, figure 3.10b illustrates that the maximum surface area for all three fluids are roughly the same; the slightly lower maximum surface area is only because the curve for intermediate density has less fluctuations.

Figure 3.10b shows that the initial spreading is not influenced at all by the density; all plots follow the same curve during the first microsecond. After that, the low density droplet spreads out slightly further, but the simulations keep roughly the same trend during the until t = 5 µs. The decrease in surface area of these droplets show a more distinct difference. This decrease can only be caused by the infiltration of fluid, so it can be postulated that only the infiltration is influenced by density, whereas spreading is not influenced at all.

However, the differences between infiltration rates are very small compared to most other simulations, which becomes clear from figure 3.7. It can be concluded that an increasing density will have a very minor impact on the behaviour of small droplets when they are infiltrating the paper coating layer.

According to the studies by Schoelkopf et al. (2000) and Ridgway and Gane (2002), an increase in density may result in inertial delay, where the acceleration of the liquid when it enters a new pore is counteracted by its inertia. However, these studies found that this effect is most pronounced for infiltration into large pores. The pore sizes in the coating that is used here are very fine; the mean pore size is 180 nm (Aslannejad et al., 2017). Therefore, this effect of inertial delay is almost negligible compared to for example viscous drag.

4.1.7 Impact velocity

When the droplet at the surface has a velocity of 5 m/s, the infiltration rate is slightly higher and the time until the maximum surface area is reached is slightly lower compared to a sessile (velocity = 0 m/s) droplet. A clear comparison between the infiltration rates of both droplets can be found in figure E.2. During the first moments, the relative water content increases faster for the case with an impact velocity: after the first timestep, at 0.5 µs, the water content is twice as high. After 2 µs, this droplet starts to behave the same as the sessile droplet and the two plots remain parallel until the droplets are fully imbibed. However, because the initial movement is faster for the droplet with an impact velocity, the 5 m/s - droplet is slightly sooner infiltrated. Therefore, the time for evaporation of the droplet at the surface is limited by the impact velocity. This is undesirable since the ink fixation will improve when the droplet resides longer at the paper surface and has more time to evaporate.

The exact same phenomenon occurs for the surface spreading. Figure 3.11b shows that the initial spreading for the droplet with a velocity of 5 m/s is significantly faster compared to a sessile droplet. However, after 1 µs, this effect tapers off and the increase and decrease of the wetted surface area remains similar to that

of a sessile droplet. The initial velocity was set in OpenFOAM in the direction perpendicular to the paper surface, hence it is interesting to see that this velocity also influences the lateral spreading.

The effect of an impact velocity on the spreading rate also influences the maximum wetted surface area, which is 0.03 μm^2 higher compared to that of water. This is a considerably large effect compared to the other simulations in this parameter study. On the contrary, the infiltration depth is exactly the same in the simulation with a sessile water droplet and a droplet with an initial velocity.

The results show that velocity of the falling droplet will influence the initial rate of spreading and infiltration, but this effect will be canceled out after a short period due to forces that inhibit the fluid flow, like viscous drag or retardation due to surface tension. These forces have a larger effect on the infiltration, compared to the surface spreading, because surface spreading is a much faster process. This explains why the wetted surface area of the droplet with an impact velocity is higher, but the infiltration depth in both simulations is the same.

On a side note, in this simulation, the droplet did not fall onto the paper and was assumed to be a perfect sphere at the moment that it touches the paper. In reality however, the droplet may deform during its fall and not arrive as a sphere. Moreover, the velocities upon arrival were also reported to be higher in some studies (Desie et al., 2004; Daniel and Berg, 2006). To better understand the influence of a falling droplet, the simulation should be repeated with other velocities.

4.2 Water and ink-like liquid

The main aim of this study is to distinguish in what way the fluid properties of an aqueous ink influence the final print on a coated paper. The difference between the final imprint of a water and ink-like liquid droplet is shown in figure 3.6, which illustrates that a change in fluid properties has hardly any effect on the distribution of fluid. However, it also shows that shape of the imprint of a droplet can still be different when the maximum distances in three directions are the same. For example, the spread in x-direction for an ink-like droplet (the middle right image in figure 3.6) more parabolic compared the the spread of a water droplet (middle left).

The previous sections clearly indicated that mainly the speed of the process is influenced by the fluid properties. This is especially true for an aqueous ink; the plot of an ink-like fluid in figure 3.7 shows the slowest infiltration rate except for the infiltration of a highly viscous fluid. This slow imbibition is a desirable effect, since it will mean that there is more time for the evaporation of the droplet at the surface. The droplet will evaporate before it is fully infiltrated, so the dye or pigments within the ink will be fixed closer to the surface, which will result in a more clear image.

It has been shown that the infiltration rate decreases for a lower surface tension, higher viscosity and higher density. The ink-like droplet has a viscosity and density that is lower compared to the intermediate viscosity and density simulations, but the infiltration rate of an ink-like liquid is lower compared to the intermediate density and viscosity simulations. Moreover, the surface tension of the ink-like liquid is equal to the surface tension that is tested in a seperate simulation. Still, the ink-like liquid infiltrates more slowly. This means that the effects that these fluid properties have on the rates of infiltration will be combined.

As explained in the introduction of this thesis, the best results in inkjet printing are achieved when there is little and slow spreading and infiltration. Much spreading at the paper surface will result in resolution loss of the final image. Increased

infiltration may cause the pigments or dye to move to far into the paper, so more ink will be needed to create a clear image at the paper surface. Slower rates of infiltration and spreading will leave more time for evaporation at the surface and the pigments/dye will also remain at the paper surface. The results of the parameter study have shown that especially the higher viscosity and lower surface tension provide desirable effect on the final ink imprint, since these properties decrease the infiltration rate. Moreover, an increase in contact angle will produce good results, because the maximum infiltration and spreading area will decline and the infiltration rate will decrease.

4.3 Technical discussion OpenFOAM

In this section, some shortcomings and possible improvements of the OpenFOAM model will be discussed. There are some inaccuracies that should be noted, as they might have influenced the results. First of all, the velocities close to the two-phase interface are really high. These velocities are caused by numerical instabilities and are called 'spurious currents' (Deshpande et al., 2012). Related to this are the really short times that are reported to reach complete droplet infiltration.

Besides, the model validation showed that the results will be influenced by the local pore structure and that the final imprint at another location at the same coating will be different. Therefore, the simulations should be repeated several times at different locations to eliminate the effect of coating properties on the results.

Moreover, evaporation is not incorporated, but it could largely influence the behaviour of the impinging droplet. First of all, it will be interesting to know whether evaporation starts to play a role after a droplet has infiltrated the paper coating, or if evaporation will also reduce the volume that is available to spreading and infiltration. Both theories are discussed in literature; Markicevic and Navaz (2010) assume that evaporation takes place after the droplet is fully infiltrated, although capillary wetting inside the paper could still coexist with evaporation. This was also shown in experiments with pL-sized droplets done by Oko et al. (2011). Experimental data of Tåg et al. (2010) indicate that evaporation could start to play a role before the droplet is fully imbibed, for example when a fast evaporating liquid is used, like alcohol. If evaporation immediately starts to compete with spreading and infiltration, this could mean that final shape of the imprint of ink in this model will be altered.

The only parameter that has a significant impact on the imprint inside and on top of the coating, was the contact angle. This was assumed to be a static value at every point where the interface between water and air was in contact with a solid surface. However, it is extensively discussed in literature that the contact angle changes during movement of a liquid; e.g. the spreading and shrinking of a droplet on a porous surface. (Gambaryan-Roisman, 2014; Brutin and Starov, 2018). To account for this, a dynamic contact angle could be implemented, where both an advancing and receding contact angle are used.

There are also some simplification made to the model to decrease the computational demand. However, these simplifications can lead to errors or unrealistic results. To improve, the following alterations could be made:

- A larger droplet size. It has been shown that the movement of fluid of the small droplet can be obstructed by the occurrence of a large pore (see figure 3.4), while the larger droplet is less influenced by pore structure. Moreover, the droplet sizes that are generally used in inkjet printing are significantly

larger; the smallest droplets that now could be created have a radius of 6 - 8 µm (Derby, 2010; Kettle et al., 2010).

- A finer mesh size. In this model, the largest cells are 60x60x60 nm, which is still relatively coarse. A grid convergence study should be carried out to determine whether the model output is independent on the grid size or if a finer base mesh should be used.
- A full droplet, instead of a quarter droplet. In the section on droplet position (section 4.1.1) it was already discussed that a droplet does not spread perfectly radial and that the local pore structure influences whether fluid will spread in a certain direction or not. This means that the behaviour in all other directions might also be different and the assumption that a quarter droplet can be used to define the behaviour of a full droplet is not realistic.
- A larger FIB-SEM image of the paper coating. The sample is now duplicated to have infiltration far away from the model boundaries. This works well enough in the case of 2 µm droplets, because the fluid does not reaches the 'seams' of the duplicated structure. However, when the droplet size becomes larger, it is better to use a larger sample without duplication.
- Run the simulations for an even longer period. In this study, the simulation is stopped shortly after the droplet was fully imbibed by the coating, to limit the total runtime. It was assumed that the distribution of the fluid inside the coating was immobile at this moment. However, there are some indications that this may not be the case. For example, the plot of infiltration depth over time of the density simulations (figure 3.10a) show that the high and low density runs reached the same infiltration depth, but the intermediate density simulation is terminated before it reaches this point. Letting a simulation run for a much longer period would solve this issue. However, that would also mean that there is a longer period during which evaporation could take place.

4.4 HYDRUS

In this section, the results of the HYDRUS simulations will be discussed.

4.4.1 Experiments

The infiltration of a large droplet (r = 20 µm) will be compared with the experimental data. The experiments are done on a coated paper, meaning that the fibrous layer was also present. It would be best to use the simulation containing a coating and the fibrous layer to compare the results to the experimental data. However, as explained in section 2.3.2, the large difference in hydraulic properties of both layers results in an initial high water content of the coating when both layers are present in the same model. Therefore, the case where only a coating is present will also be used to compare with the experimental data.

Figures 3.14 and 3.15b show that after 0.00024 seconds, the water has reached the bottom of the coating (at 12 µm) in the simulation with the coating only. One timestep later, at 0.00032, the area beneath the droplet is almost fully saturated. This is different from the observations from the experiments. The maximum infiltration depth in the experiments is in ranging between 5.5 - 11 µm (see table 2.2) and it does not reach the fibrous layer. The lateral spread also differs from the experiments: 59

µm in HYDRUS versus 15 - 25 µm in the experiments. Figure 3.13a shows an increase in infiltration flux, around 0.0005 seconds, while the flux into the coating and fibers keeps decreasing. The water balance error of the coating only simulation starts to increase at the same time. Therefore, the results of this simulation are probably incorrect and the infiltration into the coating and fibers is assumed to be more accurate. However, the duration of droplet infiltration of both simulations is still very similar, so the impact of a higher error is still low.

The simulation with the fibrous layer also shows that the coating below the droplet becomes saturated quickly. Furthermore, the water content in the fibrous layer below the droplet starts to slightly increase after 0.0012 seconds. Due to the increase in water pressure inside the coating layer during droplet infiltration, the capillary pressure (this is the macro-scale capillary pressure) decreases at the interface such that the pressure ultimately becomes low enough that the water could infiltrate the fibrous layer. The final wetted radius in this simulation (67 µm) is even higher compared to the coating-only-simulation (59 µm). This is probably due to the higher initial water content in the coating in this simulation. Since the lateral spread according to the experiments should be low, this is an indication that the initial water content in this simulation is too high.

It should be noted that evaporation is not taken into account in the HYDRUS model. This could explain why the infiltration extent in vertical and lateral direction is higher compared to the experiments. During the experiments, the droplet may have slightly evaporated when it was still at the paper surface. Also evaporation from the coating could have started when the droplet was not fully imbibed, although there are studies that report that evaporation only starts after the droplet is fully inside the paper (Markicevic and Navaz, 2010; Rahimi et al., 2016).

Both simulations show that a large region of the total imprint is unsaturated. This is due to the fact that Richards equation (equation 2.6) is a diffusive equation, where the diffusivity increases when $\delta h / \delta \theta$ increases. This gradient is very high, because the initial water content is very low, and the pressure differences close to the constant head boundary is very large and thus the diffusivity is large. Since the experiments do not show such high diffusivity, this indicates that Richards equation may be not suitable to use for this process.

In the coating+fibers simulation, the interface between the two layers is straight, with a coating layer of constant thickness. However, earlier study has shown that the coating layer is actually varying in thickness and that often single fibers are embedded in the coating (Aslannejad et al., 2018a). Moreover, fibers are found to be highly hydrophilic, so when they get in contact with the wetting fluid, the water or ink will start to flow through the fiber, while it will take longer before the pore space in between the fibers starts to fill (Aslannejad and Hassanizadeh, 2017). Since the simulation in HYDRUS does not account for the irregular interface and hydrophilicity of single fibers, the results that infiltration as shown in section 3.2.3 are assumed to be not representative of the expected behaviour.

4.4.2 Continuum-scale versus pore-scale modelling

The simulation with a wetted radius of 3 µm is used to compare the results of HYDRUS with the results of OpenFOAM. There are several differences. First of all, the infiltration depth in HYDRUS (5.528 µm) is twice the the depth in OpenFOAM (2.776 µm). However, figure 3.17b shows that the saturation inside the HYDRUS model decreases from a depth of around 2 µm, so in this case, the diffusivity is also high. The saturation in OpenFOAM cannot be derived directly, but the unsaturated area seems

signifcantly less compared to the HYDRUS results. Also, the maximum infiltration in OpenFOAM is the absolute distance measured from the paper surface, so even if the imprint in OpenFOAM was also very unsaturated, the infiltration depth is still much smaller than seen in HYDRUS. It can be concluded that the continuum-scale model assumes the water to infiltrate much further compared to the pore-scale model.

In lateral direction, the imprints in the OpenFOAM and HYDRUS runs are also different. The maximum distance in HYDRUS is 8.148 µm, which occurs at the paper surface. However, figure 3.17a indicates that the fully saturated part only slightly exceeds the original droplet radius, but that the unsaturated section increases over time. In OpenFOAM, the droplet first reaches a maximum radius of 4.2 µm at the paper surface, after which the droplet base at the paper surface starts to decrease. Inside the coating, the water reaches even further beyond the maximum droplet base at the surface due to capillary action. As a result, the maximum extent in lateral direction is 5.1 and 6.5 µm in x- and z-direction. The droplet base in HYDRUS is fixed and therefore does not show the change in wetted surface area that is illustrated in the OpenFOAM model, although the spread through the paper coating reaches the furthest at the paper surface. Moreover, the capillary action that causes lateral spread beyond the droplet radius is not reflected in the continuum-scale model.

The OpenFOAM results are influenced by local differences in pore structure. The fine pores enhance the capillary action, but if they are too fine the flow could be inhibited by viscous drag. Infiltration in large pores is inhibited by inertia and slow down the capillary action. In the previous section, it is shown that this could cause the droplet to not spread perfectly radial over the paper surface. Also, the imprint inside the coating is not symmetrical in every direction, but rather follows a path of the most optimal pore sizes. This was also an important finding in the study of Ridgway and Gane (2002) and Ridgway et al. (2002). The heterogeneity in spreading through the coating is also shown with a pore-network model that used the same hydraulic properties that are used for the HYDRUS simulations (Yin et al., 2018). However, since there are no local heterogeneities incorporated in the the use of hydraulic properties in HYDRUS, the effect of local differences in pore structure is lost.

HYDRUS may be suitable when regarding a relatively homogeneous porous medium, because the pore structure may not have a large imprint on the final distribution of water. A disadvantage when using OpenFOAM is that it is not feasible to repeat the droplet infiltration at many locations, since it will take a lot of time. In that case the water distribution will be influenced when the droplet encounters a heterogeneity in the pore structure, even if the structure is relatively homogeneous. The results of HYDRUS will then provide a more generally applicable result.

To conclude, the imprint in vertical and lateral direction is further than seen in the experiments and the result of OpenFOAM. The diffusivity of the results in HYDRUS and the absence of evaporation could be an explanation for this discrepancy. The use of a straight interface between the coating layer and fibrous layer and a constant thickness of the coating make HYDRUS unsuitable to use for infiltration in a complete coated paper. However, the infiltration into the coating layer only was also not comparable with the experimental data and results in OpenFOAM. Mainly the lack of a description of local differences in pore structure and the incapability to have a changing contact radius of the droplet at the surface causes the model in HYDRUS be significantly less accurate than OpenFOAM. Especially the latter is an important shortcoming of HYDRUS when regarding droplet infiltration for inkjet printing: the behaviour at the surface will especially influence the final quality of the printed image. Even though the results in OpenFOAM are very limited due to

the high computational demand of one simulation, it can be concluded that the use of a pore-scale model is significantly better than using a continuum-scale model.

4.5 Future research

Although this thesis has illustrated the effect of some fluid properties on the infiltration and spreading of small droplets in the paper coating layer, there are still parts that need further research.

First of all, incorporating the effect of evaporation will vastly improve the results. Evaporation is an important factor that determines the quality of the printed dot: it could counteract the spreading over the surface and reduce the possibility of bleeding. It also could prevent smearing of the drop, when the fluid does not infiltrate quick enough.

Moreover, in this study, it is assumed that the colouring is applied at every contact of the fluid with the coating. However, in a real ink, dye or pigments are added to the ink, which are possibly not reaching the same parts as the solvents of the ink. If this is the case, the coloured imprint will differ from the imprint as discussed in this study. For both dye- and pigment based inks, there are studies that show that the imprint will differ from the imprint of only the solvent part of an ink. Generally, the colourant part will adhere to the paper surface, while the solvent moves further into the coating. In the case of pigments, the particles can clog pores and are able to significantly alter the spreading and infiltration behaviour of the rest of the fluid (Desie et al., 2004; Kettle et al., 2010).

It would be interesting to compare the results of this study with the behaviour of fluids on other type of coatings. Previous studies have shown numerically and experimentally that parameters like the pore size distribution, porosity the coating structure has a large impact on the rate of infiltration and shape of final imprint (Schoelkopf et al., 2000; Ridgway and Gane, 2002; Koivula et al., 2012). Moreover, the effect of the pore structure can be different when fluids with different properties are used (Ridgway and Gane, 2002; Ridgway et al., 2002; Rahimi et al., 2016). This indicates that research on the combination of changing fluid properties and changing properties of the paper substrate is important.

Furthermore, adding a fibrous layer below the coating would be interesting. Experiments by Liu et al. (2017) show that the fibers of uncoated paper show a different infiltration pattern, as the water initially spreads along the surfaces of the fibers before entering the fibers itself and the larger pores in between. Aslannejad et al. (2018b) shows the results of a droplet infiltrating a fibrous layer, which indicates that the movement of fluid inside a fibrous layer is different compared to the behaviour in a calcite coating. Moreover, the interface between the coating layer and fibrous layer is very irregular (see the FIB-SEM image in figure 1.2) and fibers could point through the baseline of the coating layer (Aslannejad et al., 2018a). Although the aim is to keep all liquid inside the paper coating to prevent undesirable situations like the swelling of fibers, it is still possible that the ink reaches a fiber due to this irregular interface (Aslannejad et al., 2018a). However, the pore structure of the two layers is very different, so it will be a challenge to incorporate both into a pore-scale model.

5 Conclusion

In this study, the imbibition of small droplets into the thin coating layer of paper is studied by using two types of numerical models. The first model is a pore-scale model, in which FIB-SEM images of an actual paper coating layer are used to create a domain that could be used in OpenFOAM. The other model is a continuum-scale model, in which the hydraulic properties of the same coating layer and the properties of the fibrous layer of a coated paper are implemented (Aslannejad and Hassanizadeh, 2017; Aslannejad et al., 2017). The continuum-modelling is carried out with the use of the software HYDRUS.

The results of both models are compared with measurements of droplets that have infiltrated in the same coating. The droplet volume that was used in the experiments was higher than the volume that was possible to use in OpenFOAM. However, some satellite droplets were formed due to the impact of the falling droplet in the experiments. The infiltration depth and spreading extent of the droplet with a radius of 3 µm in OpenFOAM was comparable with imprint of the satellite droplets.

The results of the simulations in HYDRUS were different from the experimental data and the results of OpenFOAM. The values of infiltration depth and maximum spreading of the HYDRUS cases were much higher than in the experiments and OpenFOAM simulations. The use of Richards equation yields a highly diffuse imprint, where a large unsaturated zone occurs around the saturated part of the droplet imprint. This diffusivity, together with he inability to implement a dynamic droplet base at the paper surface and the lack of a precise description of pore structure make the HYDRUS model unfit to use for the complex process of imbibition of small droplets. Especially in the framework of inkjet printing, the behaviour of droplets at the paper surface is very important. Therefore, it is concluded that pore-scale modelling is a much better option to model these processes and a continuum model is unable to produce acceptable results.

The results of the OpenFOAM simulations show that the fluid properties have very little impact on the final distribution of ink on top and inside the paper coating. The only cases that resulted in a significantly different imprint had different values for the contact angle. Since the surface tension for these cases was kept the same, the change in contact angle reflects a change in wettability of the coating.

The rates of spreading and infiltration are influenced by several fluid properties. Increasing the viscosity resulted in the most pronounced retardation of spreading and infiltration. Decreasing the surface tension by half (but keeping the same contact angle) also resulted in a retardation of both processes. Increasing the density had a very minor effect on the infiltration rate and did not influence the rate of spreading.

When the droplet had an initial velocity at the start of the simulation, the maximum wetted surface area increased somewhat, but the infiltration depth remained the same. The rate of spreading increased slightly and the infiltration rate was only increased during the first timesteps.

This study showed that the final distribution of fluid inside the paper coating layer changed the most when comparing the simulations at different positions at the coating layer and for different contact angles. This means that the properties and

structure of the porous medium, have a large impact on the ink distribution inside a paper coating. However, this was not explicitly studied in this research, so the exact effect of the pore structure should be studied in other research.

During printing, the best quality is achieved when the ink spreads as little as possible. Moreover, the ink should stay relatively close to the paper surface, to fix the pigments and dye at the paper surface without needing too much ink and to make sure that the ink does not reach the fibrous layer. To achieve this, infiltration has to be slow to enhance evaporation so the ink pigments/dye will be fixed at the paper surface. It can be concluded that decreasing the viscosity, increasing the surface tension and increasing the contact angle will produce the best results with regard to inkjet printing of small droplets. Moreover, decreasing the impact velocity and increasing the density will have a minor, but favorable, effect.

A OpenFOAM settings

A.1 ControlDict

```
application     interFoam;

startFrom       latestTime;

startTime       0;

stopAt          endTime;

endTime         2.5e-5;

deltaT          1e-11;

writeControl    adjustableRunTime;

writeInterval   5e-7;

purgeWrite      0;

writeFormat     binary;

writePrecision  7;

writeCompression uncompressed;

timeFormat      general;

timePrecision   6;

runTimeModifiable yes;

adjustTimeStep  yes;

maxCo           0.7;
maxAlphaCo      0.7;

maxDeltaT       1;
```

Note that endTime will be changed according to the duration of the droplet infiltration and can differ for every simulation run.

A.2 fvSolution

```
solvers
{
    "alpha.water.*"
    {
        nAlphaCorr      2;
        nAlphaSubCycles 1;
        cAlpha          0.8;

        MULESCorr       yes;
        nLimiterIter    3;

        solver          PBiCG;
        preconditioner  DILU;
        tolerance       1e-8;
        relTol          0;
    }

    pcorr
    {
        solver                  PCG;
        preconditioner          DIC;
        tolerance               1e-06;
        relTol                  0;
    }

    pcorrFinal
    {
        $pcorr;
    }

    p_rgh
    {
        solver                  PCG;
        preconditioner          DIC;
        tolerance               1e-06;
        relTol                  0;
    }

    p_rghFinal
    {
        $p_rgh;
    }

    U
    {
        solver          PBiCG;
        preconditioner  DILU;
        tolerance       1e-06;
        relTol          0;
    }

    UFinal
    {
        $U;
    }
}

PIMPLE
{
    momentumPredictor   no;
    nOuterCorrectors    1;
    nCorrectors         2;
    nNonOrthogonalCorrectors 1;
}

relaxationFactors
{
    equations
    {
        ".*" 1;
    }
}
```

A.3 fvSchemes

```
ddtSchemes
{
    default Euler;
}

gradSchemes
{
    default         Gauss linear;
}

divSchemes
{
    div(rhoPhi,U)  Gauss upwind;
    div(phi,alpha)  Gauss vanLeer;
    div(phirb,alpha) Gauss linear;
    div(((rho*nuEff)*dev2(T(grad(U))))) Gauss linear;
}

laplacianSchemes
{
    default         Gauss linear corrected;
}

interpolationSchemes
{
    default         linear;
}

snGradSchemes
{
    default         corrected;
}
```

B OpenFOAM mesh files

B.1 BlockMeshDict

```
convertToMeters 1e-9;

vertices
(
    (1600 6 1)
    (6000 6 1)
    (6000 7125 1)
    (1600 7125 1)
    (1600 6 4400)
    (6000 6 4400)
    (6000 7125 4400)
    (1600 7125 4400)
);

blocks
(
    hex (0 1 2 3 4 5 6 7) (73 119 73) simpleGrading (1 1 1)
);

edges
(
);

boundary
(
    Up
    {
        type patch;
        faces
        (
            (3 7 6 2)
        );
    }

    Down
    {
        type patch;
        faces
        (
            (1 5 4 0)
        );
    }

    Right
    {
        type symmetryPlane;
        faces
        (
            (2 6 5 1)
        );
    }

    Left
    {
        type patch;
        faces
        (
            (0 4 7 3)
        );
    }

    Front
    {
        type patch;
        faces
        (
            (0 3 2 1)
        );
    }

    Back
    {
        type symmetryPlane;
        faces
        (
            (4 5 6 7)
        );
    }

);

mergePatchPairs
(
);
```

B.2 SnappyHexMeshDict

```
castellatedMesh true;
snap            true;
addLayers       false;

geometry
{
    STL.stl
    {
        type    triSurfaceMesh;
        name    coating;
        scale   1e-9;
    }
};

castellatedMeshControls
{
    maxLocalCells 3000000;
    maxGlobalCells 50000000;
    minRefinementCells 20;
    nCellsBetweenLevels 2;

    features ();

    refinementSurfaces
    {
        coating
        {
            level (1 1);
        }
    }
    resolveFeatureAngle 30;

    refinementRegions
    {
    }

    locationInMesh (5e-6 4e-6 3e-6);
    allowFreeStandingZoneFaces true;
}


snapControls
{
    nSmoothPatch 3;
    tolerance 4.0;
    nSolveIter 10;
    nRelaxIter 5;
}

addLayersControls
{
}

meshQualityControls
{
    maxNonOrtho 65;
    maxBoundarySkewness 4;
    maxInternalSkewness 4;
    maxConcave 80;
    minVol -1e30;
    minTetQuality 1e-30;
    minArea -1;
    minTwist 0.05;
    minDeterminant 0.001;
    minFaceWeight 0.05;
    minVolRatio 0.01;
    minTriangleTwist -1;
    nSmoothScale 1;
    errorReduction 0.75;
}

mergeTolerance 1e-6;
```

C OpenFOAM boundary conditions

In this appendix, the input for the files alpha.water, velocity and pressure is shown. These files contain information on the boundary conditions that will be used and are stored in the *0*-folder of the OpenFOAM case. The dimensions are stored as SI units in the following way: dimensions [kg m s K mol A cd]. For example, the dimensions of velocity are stored as dimensions [0 1 -1 0 0 0 0], which corresponds to m/s.

C.1 Alpha.water

```
dimensions      [0 0 0 0 0 0 0];

internalField   uniform 0;

boundaryField
{
    Up
    {
        type            zeroGradient;
    }
    Down
    {
        type            inletOutlet;
        inletValue      uniform 0;
        value           uniform 0;
    }
    Right
    {
        type            symmetryPlane;
    }
    Left
    {
        type            inletOutlet;
        inletValue      uniform 0;
        value           uniform 0;
    }
    Front
    {
        type            inletOutlet;
        inletValue      uniform 0;
        value           uniform 0;
    }
    Back
    {
        type            symmetryPlane;
    }
    coating
    {
        type            constantAlphaContactAngle;
        theta0          45;
        limit           gradient;
        value           uniform 0;
    }
}
```

C.2 Velocity

```
dimensions      [0 1 -1 0 0 0 0];

internalField   uniform (0 0 0);

boundaryField
{
    Up
    {
        type            fixedValue;
        value           uniform (0 0 0);
    }
    Down
    {
        type            pressureInletOutletVelocity;
        value           uniform (0 0 0);
    }
    Right
    {
        type            symmetryPlane;
    }
    Left
    {
        type            pressureInletOutletVelocity;
        value           uniform (0 0 0);
    }
    Front
    {
        type            pressureInletOutletVelocity;
        value           uniform (0 0 0);
    }
    Back
    {
        type            symmetryPlane;
    }
    coating
    {
        type            fixedValue;
        value           uniform (0 0 0);
    }
}
```

C.3 Pressure (p_rgh)

```
dimensions      [1 -1 -2 0 0 0 0];

internalField   uniform 0;

boundaryField
{
    Up
    {
        type            fixedFluxPressure;
        gradient        uniform 0;
        value           uniform 0;
    }
    Down
    {
        type            totalPressure;
        rho             rho;
        psi             none;
        gamma           1;
        p0              uniform 0;
        value           uniform 0;
    }
    Right
    {
        type            symmetryPlane;
    }
    Left
    {
        type            totalPressure;
        rho             rho;
        psi             none;
        gamma           1;
        p0              uniform 0;
        value           uniform 0;
    }
    Front
    {
        type            totalPressure;
        rho             rho;
        psi             none;
        gamma           1;
        p0              uniform 0;
        value           uniform 0;
    }
    Back
    {
        type            symmetryPlane;
    }
    coating
    {
        type            fixedFluxPressure;
        gradient        uniform 0;
        value           uniform 0;
    }
}
```

D HYDRUS settings

D.1 Spatial discretization

All mesh and geometry settings are specified in table D.1. To improve the stability of the model, the cells at the paper surface should be small, therefore a relative size is specified. This size is specified in the last column of table D.1. A value of 0.1 means that the surface cells are ten times smaller than the cells at the bottom. The rest of the cells are changed to get a gradual change in cell size from top to bottom.

TABLE D.1: Mesh and geometry information. Spatial discretization describes the number of nodes in one direction

	Length (x) [µm]	Spatial discretization (x)	Depth (z) [µm]	Spatial discretization (z)	Relative size of top cells
Coating+fibers	300	360	Coating: 12 Fibers: 61	90	0.1
Coating only					
3 µm droplet	20	55	12	120	0.2
20 µm droplet	100	200	12	45	0.1

D.2 Time discretization and iteration criteria

All settings regarding the time discretization and iteration process are listed in table D.2.

TABLE D.2: Settings regarding time discretization and iteration

	Coating + fibers	**Coating + 3 µm droplet**	**Coating + 19 µm droplet**
Initial time step [s]	1e-7	1e-9	1e-9
Minimum time step [s]	1e-9	1e-11	1e-11
Maximum time step [s]	1	1	1
Maximum number of iterations	10	10	10
Water content tolerance	5e-7	5e-7	1e-6
Pressure head tolerance	0.0001	0.0001	0.001
Lower optimal iteration range	3	3	3
Upper optimal iteration range	7	7	7
Lower timestep multiplication factor	1.3	1.3	1.3
Upper timestep multiplication factor	0.7	0.7	0.7
Internal interpolation tables	Disabled	Disabled	Disabled

E Results OpenFOAM

E.1 Infiltration plots

Below, the relative water content plot showing all results of the parameter study (figure 3.7) is split into several plots to compare the effect of a change in a single property.

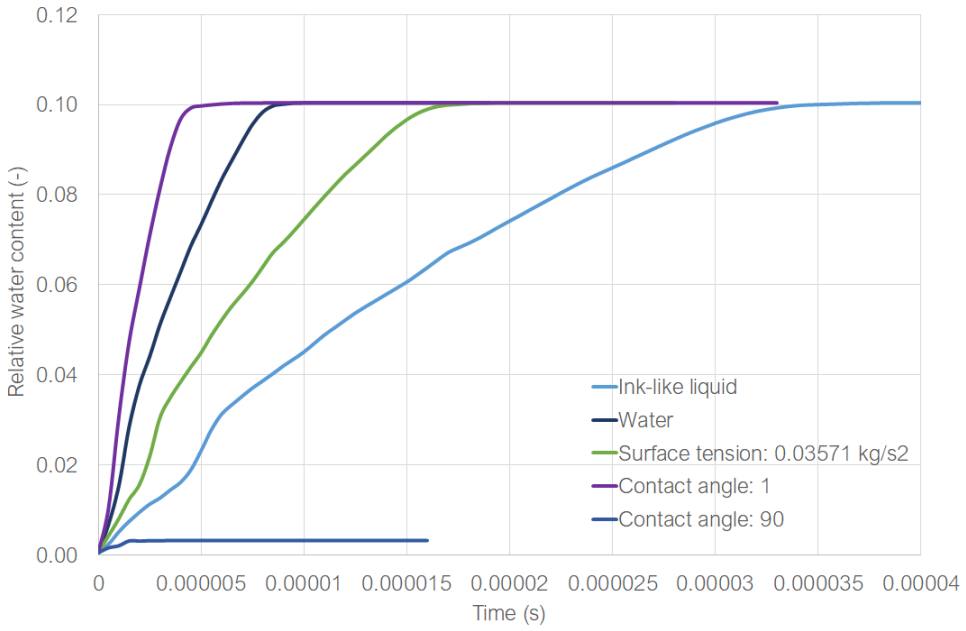

FIGURE E.1: Relative water content of water, ink, surface tension and both contact angle simulations

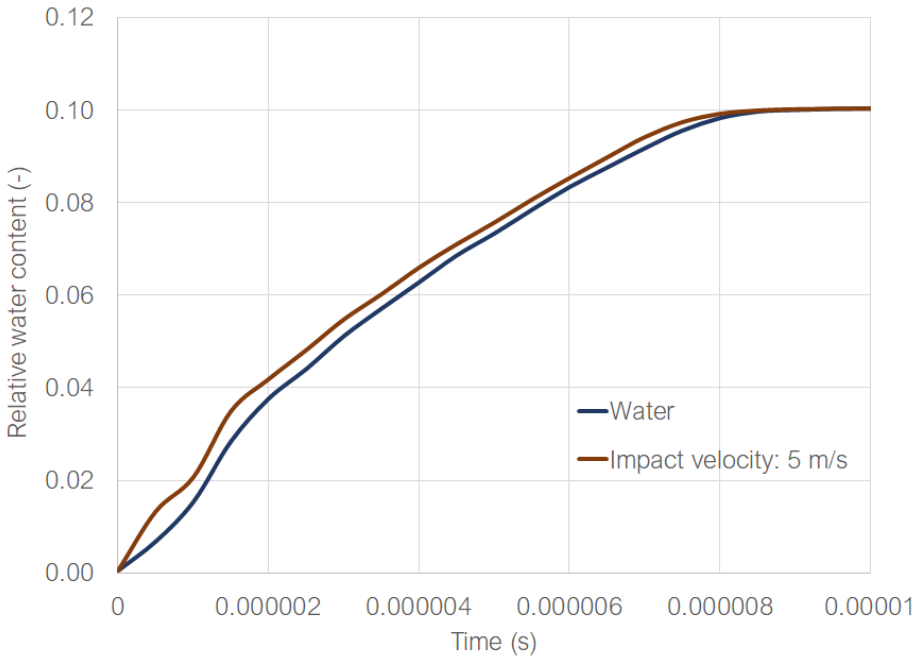

FIGURE E.2: Relative water content of a sessile droplet (water) and a droplet with velocity of 5 m/s

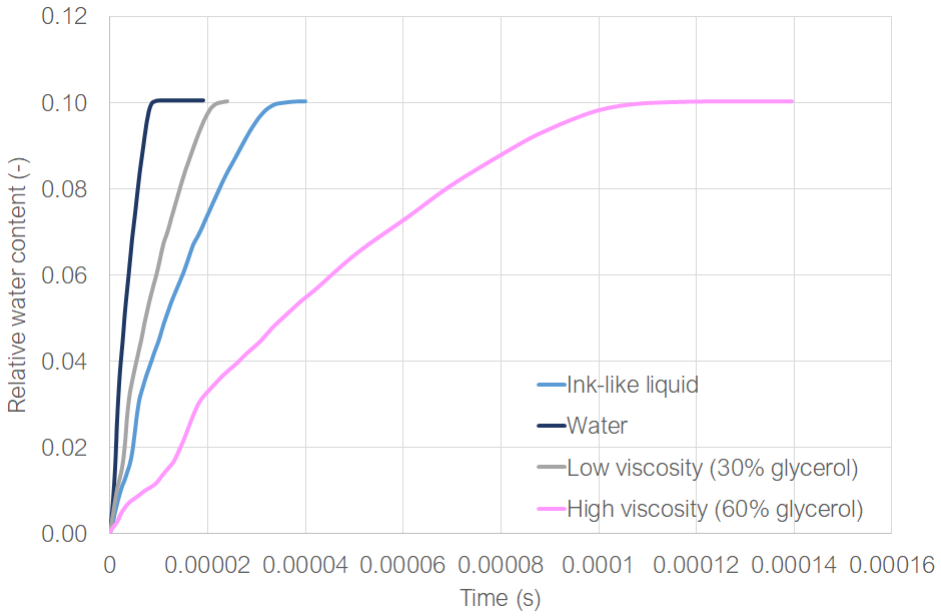

FIGURE E.3: Relative water content of water, ink and both viscosity simulations

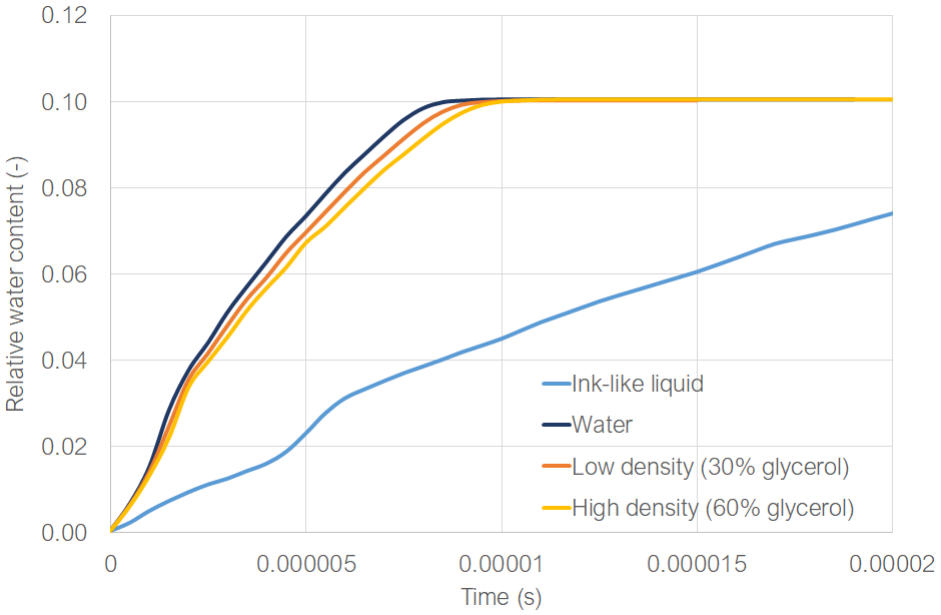

FIGURE E.4: Relative water content of density simulations. The graph of the ink-like liquid is cut off to zoom in at the density simulations

Bibliography

Alleborn, N. and H. Raszillier (2004). "Spreading and sorption of a droplet on a porous substrate". In: *Chemical Engineering Science* 59.10, pp. 2071–2088.

Aslannejad, H. and S.M. Hassanizadeh (2017). "Study of hydraulic properties of uncoated paper: image analysis and pore-scale modeling". In: *Transport in Porous Media* 120.1, pp. 67–81.

Aslannejad, H., S.M. Hassanizadeh, A. Raoof, D.A.M. de Winter, N. Tomozeiu, and M.Th. van Genuchten (2017). "Characterizing the hydraulic properties of paper coating layer using FIB-SEM tomography and 3D pore-scale modeling". In: *Chemical Engineering Science* 160, pp. 275–280.

Aslannejad, H., S.M. Hassanizadeh, and M.A. Celia (2018a). "Characterization of the Interface Between Coating and Fibrous Layers of Paper". In: *Transport in Porous Media*, pp. 1–13.

Aslannejad, H., H. Fathi, S.M. Hassanizadeh, A. Raoof, and N. Tomozeiu (2018b). "Movement of a liquid droplet within a fibrous layer: Direct pore-scale modeling and experimental observations". In: *Chemical Engineering Science* 191, pp. 78–86.

Ayachit, U. (2015). *The ParaView Guide: A Parallel Visualization Application*. Version 5.4.

Bahr, M. von, F. Tiberg, and B. Zhmud (2003). "Oscillations of sessile drops of surfactant solutions on solid substrates with differing hydrophobicity". In: *Langmuir* 19.24, pp. 10109–10115.

Bonn, D., J. Eggers, J. Indekeu, J. Meunier, and E. Rolley (2009). "Wetting and spreading". In: *Reviews of modern physics* 81.2, p. 739.

Bosanquet, C.H. (1923). "On the flow of liquids into capillary tubes". In: *The London, Edinburgh, and Dublin Philosophical Magazine and Journal of Science* 45.267, pp. 525–531.

Brutin, D. and V. Starov (2018). "Recent advances in droplet wetting and evaporation". In: *Chemical Society Reviews* 47.2, pp. 558–585.

Cheng, N.S. (2008). "Formula for the viscosity of a glycerol- water mixture". In: *Industrial & engineering chemistry research* 47.9, pp. 3285–3288.

Daniel, R.C. and J.C. Berg (2006). "Spreading on and penetration into thin, permeable print media: Application to ink-jet printing". In: *Advances in colloid and interface science* 123, pp. 439–469.

Davis, S.H. and L.M. Hocking (1999). "Spreading and imbibition of viscous liquid on a porous base". In: *Physics of fluids* 11.1, pp. 48–57.

Derby, B. (2010). "Inkjet printing of functional and structural materials: fluid property requirements, feature stability, and resolution". In: *Annual Review of Materials Research* 40, pp. 395–414.

Deshpande, S.S., L. Anumolu, and M.F. Trujillo (2012). "Evaluating the performance of the two-phase flow solver interFoam". In: *Computational science & discovery* 5.1, p. 014016.

Desie, G., G. Deroover, F. De Voeght, and A. Soucemarianadin (2004). "Printing of dye and pigment-based aqueous inks onto porous substrates". In: *Journal of Imaging Science and Technology* 48.5, pp. 389–397.

Fathi, H., A. Raoof, and S.H. Mansouri (2017). "Insights into the role of wettability in cathode catalyst layer of proton exchange membrane fuel cell; pore scale immiscible flow and transport processes". In: *Journal of Power Sources* 349, pp. 57–67.

Fu, F., P. Li, K. Wang, and R. Wu (2019). "Numerical Simulation of Sessile Droplet Spreading and Penetration on Porous Substrates". In: *Langmuir*.

Gambaryan-Roisman, T. (2014). "Liquids on porous layers: wetting, imbibition and transport processes". In: *Current Opinion in Colloid & Interface Science* 19.4, pp. 320–335.

Järnström, J., M. Väisänen, R. Lehto, A. Jäsberg, J. Timonen, and J. Peltonen (2010). "Effect of latex on surface structure and wetting of pigment coatings". In: *Colloids and Surfaces A: Physicochemical and Engineering Aspects* 353.2-3, pp. 104–116.

Kettle, J., T. Lamminmäki, and P. Gane (2010). "A review of modified surfaces for high speed inkjet coating". In: *Surface and coatings Technology* 204.12-13, pp. 2103–2109.

Koivula, H., M. Toivakka, and P. Gane (2012). "Short time spreading and wetting of offset printing liquids on model calcium carbonate coating structures". In: *Journal of colloid and interface science* 369.1, pp. 426–434.

Lamminmäki, T., J. Kettle, H. Rautkoski, A. Kokko, and P. Gane (2011). "Limitations of current formulations when decreasing the coating layer thickness of papers for inkjet printing". In: *Industrial & Engineering Chemistry Research* 50.12, pp. 7251–7263.

Lee, H.K., M.K. Joyce, P.D. Fleming, and J. Cameron (2002). "Production of a single coated glossy inkjet paper using conventional coating and calendering methods". In: pp. 357–380.

Lim, T., S. Han, J. Chung, J.T. Chung, S. Ko, and C.P. Grigoropoulos (2009). "Experimental study on spreading and evaporation of inkjet printed pico-liter droplet on a heated substrate". In: *International Journal of Heat and Mass Transfer* 52.1-2, pp. 431–441.

Liu, G., S. Fu, Z. Lu, M. Zhang, C. Ridgway, and P. Gane (2017). "Contrasting liquid imbibition into uncoated versus pigment coated paper enables a description of imbibition into new-generation surface-filled paper". In: *The European Physical Journal E* 40.12, p. 111.

Markicevic, B. and H.K. Navaz (2010). "The influence of capillary flow on the fate of evaporating wetted imprint of the sessile droplet in porous medium". In: *Physics of Fluids* 22.12, p. 122103.

Mualem, Y. (1976). "A new model for predicting the hydraulic conductivity of unsaturated porous media". In: *Water Resources Research* 12.3, pp. 513–522.

Oko, A., P. Claesson, and A. Swerin (2011). "Imbibition and evaporation of water droplets on paper and solid substrates". In: *Journal of Imaging Science and Technology* 55.1, pp. 10201–1–6.

Rahimi, A., T. Metzger, A. Kharaghani, and E. Tsotsas (2016). "Interaction of droplets with porous structures: Pore network simulation of wetting and drying". In: *Drying technology* 34.9, pp. 1129–1140.

Ridgway, C.J. and P.A.C. Gane (2002). "Dynamic absorption into simulated porous structures". In: *Colloids and Surfaces A: Physicochemical and Engineering Aspects* 206.1-3, pp. 217–239.

Ridgway, C.J., P.A.C. Gane, and J. Schoelkopf (2002). "Effect of capillary element aspect ratio on the dynamic imbibition within porous networks". In: *Journal of Colloid and Interface Science* 252.2, pp. 373–382.

Schoelkopf, J., P.A.C. Gane, C.J. Ridgway, and G.P. Matthews (2000). "Influence of inertia on liquid absorption into paper coating structures". In: *Nordic Pulp & Paper Research Journal* 15.5, pp. 422–430.

Šimůnek, J., M.Th. Van Genuchten, and M. Šejna (2006). "The HYDRUS software package for simulating two-and three-dimensional movement of water, heat, and multiple solutes in variably-saturated media". In: 1, p. 241.

Starov, V.M., S.R. Kostvintsev, V.D. Sobolev, M.G. Velarde, and S.A. Zhdanov (2002). "Spreading of liquid drops over dry porous layers: complete wetting case". In: *Journal of colloid and interface science* 252.2, pp. 397–408.

Szymkiewicz, A. (2013). "Mathematical Models of Flow in Porous Media". In: *Modelling Water Flow in Unsaturated Porous Media: Accounting for nonlinear permeability and material heterogeneity*. Springer, pp. 9–47.

Tåg, C.M., M. Juuti, K. Koivunen, and P.A.C. Gane (2010). "Dynamic water transport in a pigmented porous coating medium: novel study of droplet absorption and evaporation by near-infrared spectroscopy". In: *Industrial & Engineering Chemistry Research* 49.9, pp. 4181–4189.

Tan, H. (2017). "Absorption of picoliter droplets by thin porous substrates". In: *AIChE Journal* 63.5, pp. 1690–1703.

Tanner, L.H. (1979). "The spreading of silicone oil drops on horizontal surfaces". In: *Journal of Physics D: Applied Physics* 12.9, p. 1473.

The Blender Documentation Team (2019). *The Blender Manual*. Version 2.79. URL: `https://docs.blender.org/manual/en/latest/`.

The OpenFOAM Foundation (2018). *OpenFOAM User Guide*. Version 6. URL: `https://cfd.direct/openfoam/user-guide`.

Van Genuchten, M. Th. (1980). "A closed-form equation for predicting the hydraulic conductivity of unsaturated soils". In: *Soil science society of America journal* 44.5, pp. 892–898.

Volk, A. and C.J. Kähler (2018). "Density model for aqueous glycerol solutions". In: *Experiments in Fluids* 59.5, p. 75.

Washburn, E.W. (1921). "The dynamics of capillary flow". In: *Physical review* 17.3, p. 273.

Yarin, A. L (2006). "Drop impact dynamics: splashing, spreading, receding, bouncing…" In: *Annu. Rev. Fluid Mech.* 38, pp. 159–192.

Yin, X., H. Aslannejad, E.T. de Vries, A. Raoof, and S.M. Hassanizadeh (2018). "Droplet Imbibition into Paper Coating Layer: Pore-Network Modeling Simulation". In: *Transport in Porous Media* 125.2, pp. 239–258.